NASA/TM-1999-209531

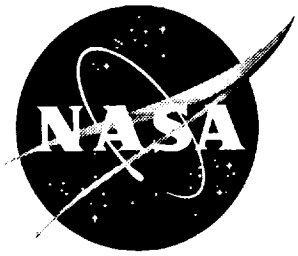

Taxiing, Take-Off, and Landing Simulation of the High Speed Civil Transport Aircraft

Mercedes C. Reaves and Lucas G. Horta
Langley Research Center, Hampton, Virginia

December 1999

The NASA STI Program Office . . . in Profile

Since its founding, NASA has been dedicated to the advancement of aeronautics and space science. The NASA Scientific and Technical Information (STI) Program Office plays a key part in helping NASA maintain this important role.

The NASA STI Program Office is operated by Langley Research Center, the lead center for NASA's scientific and technical information. The NASA STI Program Office provides access to the NASA STI Database, the largest collection of aeronautical and space science STI in the world. The Program Office is also NASA's institutional mechanism for disseminating the results of its research and development activities. These results are published by NASA in the NASA STI Report Series, which includes the following report types:

- TECHNICAL PUBLICATION. Reports of completed research or a major significant phase of research that present the results of NASA programs and include extensive data or theoretical analysis. Includes compilations of significant scientific and technical data and information deemed to be of continuing reference value. NASA counterpart of peer-reviewed formal professional papers, but having less stringent limitations on manuscript length and extent of graphic presentations.

- TECHNICAL MEMORANDUM. Scientific and technical findings that are preliminary or of specialized interest, e.g., quick release reports, working papers, and bibliographies that contain minimal annotation. Does not contain extensive analysis.

- CONTRACTOR REPORT. Scientific and technical findings by NASA-sponsored contractors and grantees.

- CONFERENCE PUBLICATION. Collected papers from scientific and technical conferences, symposia, seminars, or other meetings sponsored or co-sponsored by NASA.

- SPECIAL PUBLICATION. Scientific, technical, or historical information from NASA programs, projects, and missions, often concerned with subjects having substantial public interest.

- TECHNICAL TRANSLATION. English-language translations of foreign scientific and technical material pertinent to NASA's mission.

Specialized services that complement the STI Program Office's diverse offerings include creating custom thesauri, building customized databases, organizing and publishing research results . . . even providing videos.

For more information about the NASA STI Program Office, see the following:

- Access the NASA STI Program Home Page at ***http://www.sti.nasa.gov***

- Email your question via the Internet to help@sti.nasa.gov

- Fax your question to the NASA STI Help Desk at (301) 621-0134

- Telephone the NASA STI Help Desk at (301) 621-0390

- Write to:
  NASA STI Help Desk
  NASA Center for AeroSpace Information
  7121 Standard Drive
  Hanover, MD 21076-1320

NASA/TM-1999-209531

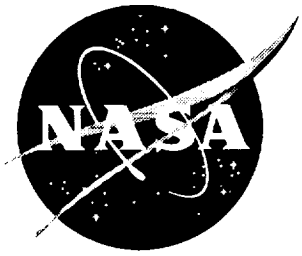

Taxiing, Take-Off, and Landing Simulation of the High Speed Civil Transport Aircraft

Mercedes C. Reaves and Lucas G. Horta
Langley Research Center, Hampton, Virginia

National Aeronautics and
Space Administration

Langley Research Center
Hampton, Virginia 23681-2199

December 1999

Available from:

NASA Center for AeroSpace Information (CASI)
7121 Standard Drive
Hanover, MD 21076-1320
(301) 621-0390

National Technical Information Service (NTIS)
5285 Port Royal Road
Springfield, VA 22161-2171
(703) 605-6000

Table of Contents

1. Introduction 2

2. Airframe Model 3

3. Equations of Motion 3

3.1 Mode Selection Approach 6

4. Landing Gear 6

4.1 Runway Model 7

5. System Integration / Numerical Simulations 8

6. Simulation Results 8

6.1 Aircraft Response During Ground Operations 8
6.2 Taxiing Simulations 9
6.3 Rejected Takeoff Simulations 9
6.4 Landing Simulations 10
6.5 Frequency Comparison of the Various Ground Operations 10
6.6 Human Response to Vibration 11

7. Concluding Remarks 11

8. References 11

9. Tables 13

10. Figures 15

1. Introduction

The High Speed Civil Transport (HSCT) has been identified as a means to extend the role of the United States as the leader in aerospace well into the 21st century. However, the unique configuration of the aircraft and its operational requirements present numerous technical design challenges. The HSCT airframe, driven by aerodynamic design constraints and design considerations, has relatively low stiffness compared to subsonic aircraft. Also, the nose gear is well aft of the flight crew deck creating a long overhang. Previous supersonic transport aircraft configurations, such as the Concorde and XB-70 aircraft, all exhibited excessive fuselage dynamic response during ground operations. [1,2] NASA Langley Research Center has initiated a research effort to assess the problem of ground-induced vibration for this new HSCT configuration. Being able to identify such a problem in the early stages of the design process will enable designers to address the problem early.

Computer simulations have been conducted to study the HSCT vibration levels during taxiing, landing, and takeoff roll-out. A linear modal math model of the airframe with no landing gear is constructed by combining the symmetric and antisymmetric modes of the airframe. The landing gear dynamics, including inertia, damping and stiffness properties, are introduced as external nonlinear forces. Software capable of detailed nonlinear simulation of an aircraft and/or its landing gear and all associated sub-systems is available [3,4] and could be used in future studies or advance design stage. In the present work SIMULINK[5] , a commercial computer simulation program, is used to numerically integrate the equations of motion and to postprocess the data. The profile for a runway at San Francisco airport (commonly used by the FAA for airplane certification) is used as input to the simulation. Displacement and acceleration time histories are obtained at the cockpit and at various fuselage and wing locations for forward speeds ranging from 30 knots to 175 knots. Although the model contains simplified landing gear system information, e.g., no specific oleo strut mechanics or dynamics (piston, metering pin, etc.) have been modeled, the simplified model of the gear, nonlinear spring and damping forces as a function of stroke, proved to be adequate to assess the vibration problem.

This document describes the aircraft configuration in terms of structural and mass models, defines the analysis approach, systems models, computer simulation, and discusses results from the simulations.

2. Airframe Model

The HSCT weights and finite element models used in this investigation are based on the Boeing HSCT 1080-920STR model E configuration, Ref. [6], with the landing gear deployed. A sketch of the aircraft, an aft tail / four engine configuration vehicle, is shown in Fig. 1 with the landing gear in the stowed position. The original finite element model created by Boeing using ELFINI[7], a general purpose FEM software package, was translated into MSC/NASTRAN[8] format using a translator developed in-house. The HSCT FEM, Fig. 2, represents the (symmetrical) right half of the aircraft and contains 38,444 degrees of freedom. This finite element model is divided into fourteen sections as shown in Figure 3. Table 1 contains a description of each section. The primary structure which is modeled consists of skins, chords, spar webs and landing gears posts, trunions and drag braces. Secondary structure, such as windows, passenger doors, access doors, etc., is not modeled because it is not necessary for strength or flutter analysis. Symmetric and antisymmetric configurations are represented by applying the appropriate boundary conditions to the degrees of freedom in the vertical plane of symmetry of the aircraft.

A data base of lumped masses representing the airplane mass distributions for the primary and secondary structures with combinations of on empty weight (OEW), payload and fuel weights were supplied by Boeing, Ref. [6]. Depending on the analysis to be conducted (e.g., flutter, ground operations, etc.) the appropriate set of lumped masses can be obtained from the data base and included in the structural finite element model as lumped mass elements at specific grid point locations. The mass cases used in this investigation are designated mass case MO5 and mass case M14, Ref. [6]. MO5 is a representation of the airplane at maximum taxi or takeoff weight of 646,454 lbf with full wing fuel and with c.g. located aft of the OEW (on empty weight) c.g. location. For landing simulation mass case M14 was selected, for a total weight of 388,584 lbf which includes the OEW, aft body full tank, and payload for an aft c.g. location. These conditions are considered the worst case scenarios for ground operations.

3. Equations of Motion

To develop dynamic models for aircraft response analysis during taxiing, take-off, and landing, it is required to combine airframe flexibility with landing gear dynamics. Airframe structure is routinely modeled using finite element model (FEM) approaches whereas landing gears are often modeled using equations obtained by semi-empirical

approaches. A finite element dynamic model of the airframe leads to a set of matrix differential equations of the form

$$M\ddot{x}(t) + Kx(t) = bu(t) \tag{1}$$

where x(t) is a response vector order n x 1, M and K are the mass and stiffness matrices, respectively, of order n x n, b is a direction cosine matrix locating external forces or moments, and $u(t)$ is a vector of applied forces or moments. The integer n is the total number of degrees-of-freedom (DOF) used to construct the model, often a very large number. For dynamic simulations it is important to reduce the size of the system in Eq. (1). Typically, modal reduction techniques are used to reduce the size of the model. One approach solves for the eigenvalues Λ^2 and corresponding eigenvectors P such that $P^T M P = I$, and $P^T K P = \Lambda^2$. Assuming that the computed eigenvector matrix can be partitioned into groups of symmetric and antisymmetric modes such that $P = [\Phi \quad \Psi]$, where Φ are the symmetric and Ψ are the antisymmetric modes, and substituting the coordinate transformation $x = P\eta$ into Eq. (1) yields a decoupled set of equations as follows

$$\begin{Bmatrix} \ddot{\eta}_s \\ \ddot{\eta}_{as} \end{Bmatrix} + \begin{bmatrix} \omega_s^2 & \\ & \omega_{as}^2 \end{bmatrix} \begin{Bmatrix} \eta_s \\ \eta_{as} \end{Bmatrix} = \begin{Bmatrix} \Phi^T b \\ \Psi^T b \end{Bmatrix} u(t) \tag{2}$$

where $\eta^T = [\eta_s \quad \eta_{as}]$ and $\Lambda^2 = diag(\omega_s^2, \omega_{as}^2)$. The subscripts 's' and 'as' refer to the symmetric and antisymmetric parts of the equation. Model reduction is accomplished by retaining only a selected number of modes, normally fewer that the total available, for analysis. So far it has tacitly been assumed that the full airplane configuration is modeled and that an eigenvalue solution is computed. However, this is not necessary if one can take advantage of symmetry, as discussed in Ref. [9]. By judiciously positioning the reference coordinate system in the vertical plane of symmetry only half of the airframe structure actually needs to be modeled, Fig. 2. The symmetrical and antisymmetrical eigenvectors and eigenvalues can be computed by imposing the boundary conditions which are consistent with the symmetry conditions. For example, the symmetric case requires the degrees of freedon in the vertical plane of symmetry to be restrained from yaw, roll and lateral translation, whereas the antisymmetric case requires restraining the degrees of freedon in the vertical plane of symmetry from vertical translation, pitch rotation, and forward translation. To recover information for the left-half of the airframe, the mode shapes are expanded according to symmetry conditions, for example, $\phi(l) = \phi(-l)$ and

$\psi(l) = -\psi(-l)$ and when combined with time histories of the generalized coordinate vector $\eta(t)$ allows computation of the airframe left-half response.

To take advantage of existing numerical integration tools, the first-order form of Eq. (2) is needed. Defining a new state vector $z = [n_s \quad n_{as} \quad \dot{n}_s \quad \dot{n}_{as}]^T$, Eq. (2) can be written in first-order form as

$$\begin{aligned}
&\dot{z}(t) = Az(t) + Bu(t) \\
&x = Cz(t) + Du(t) \\
&A = \begin{bmatrix} \underline{0} & \underline{0} & I & \underline{0} \\ \underline{0} & \underline{0} & \underline{0} & I \\ -\omega_s^2 & \underline{0} & \underline{0} & \underline{0} \\ \underline{0} & -\omega_{as}^2 & \underline{0} & \underline{0} \end{bmatrix}; B = \begin{Bmatrix} \underline{0} \\ \underline{0} \\ \Phi^T b \\ \Psi^T b \end{Bmatrix} \\
&C = [\Phi \quad \Psi \quad \underline{0} \quad \underline{0}] \\
&D = \underline{0}
\end{aligned} \tag{3}$$

where $\underline{0}$ represent a null matrix with the proper dimensions. Equation (3) allows calculation of responses in terms of the symmetric and antisymmetric modal coordinates due to arbitrary inputs to the airframe. If acceleration responses are also needed, the output vector in Eq.(3) must be augmented as follows

$$y = \begin{Bmatrix} x \\ \dot{x} \\ \ddot{x} \end{Bmatrix} = \begin{bmatrix} \Phi & \Psi & \underline{0} & \underline{0} \\ \underline{0} & \underline{0} & \Phi & \Psi \\ -\Phi\omega_s^2 & -\Psi\omega_{as}^2 & \underline{0} & \underline{0} \end{bmatrix} z(t) + \begin{bmatrix} \underline{0} \\ \underline{0} \\ \Phi\Phi^T b + \Psi\Psi^T b \end{bmatrix} u(t) \tag{4}$$

and D is not null. The equations presented so far dealt with the airframe flexibility as derived from the FEM. To incorporate landing gear dynamics, the approach is to use empirical representations of the landing gear force versus stroke response and stroke versus damping coefficient directly in the simulation. In its most general form, the landing gear forces can be conceptually represented as

$$u(t) = f(y, \dot{y}, \delta(t)) \tag{5}$$

where the newly-defined parameter $\delta(t)$ corresponds to time variation of runway elevations provided as input to the simulation program. Although Eq. (5) is deceptively simple, a significant amount of time must be devoted to the experimental characterization of the landing gear system if one expects to obtain high fidelity models using an empirical approach. Typical experimental curves for Eq.(5) are presented in a later section.

3.1 Mode Selection Approach

The symmetric and antisymmetric vibration modes of the Boeing HSCT 1080-892STR-E model with a 'rigid stick model' of the landing gear in the extended position and M05 mass distribution were calculated using MSC/NASTRAN. A customized NASTRAN/DMAP sequence was used to compute the kinetic energy associated with the vibration modes in an effort to differentiate local modes from global modes to be used in the simulations. Boeing-defined sections (fwd. fuselage, control surfaces, etc.)[10] were used to divide the model into physically meaningful sections. A sample portion of the kinetic energy results obtained for the HSCT with symmetric boundary conditions and MO5 weight distribution is shown in Table 2. Since all sections are included in the list, the total kinetic energy is 100%. Figure 4 contains contour plots of the kinetic energy for the symmetric and antisymmetric modes. Based on these results, the symmetric and antisymmetric global airframe modes with the highest kinetic energy were selected for inclusion in the mode sets Φ and Ψ .

In all, a combination of 8 symmetric modes (3 rigid modes , 5 flexible modes) and 7 antisymmetric modes (3 rigid modes and 4 flexible modes) in the frequency range between 0.0 and 6.67 Hz were chosen to represent the airframe flexibility for taxiing, takeoff and landing conditions. The flexible mode frequencies and mode shapes corresponding to equivalent modes from mass cases M05 and M14 are shown in Figures 5 through 13. The symmetric rigid-body modes represent the aircraft vertical translation, pitch rotation, and forward translation. The antisymmetric rigid-body modes represent the aircraft yaw, roll, and lateral translation. The first two flexible modes appeared at relatively low frequencies 1.3 Hz and 1.5 Hz for the symmetric and antisymmetric cases respectively, compared to 3.6 Hz for a typical commercial transport configuration, Ref. [11].

4. Landing gear

It is important to distinguish between the landing gear structural model and the landing gear dynamic model. In this document the term 'landing gear structural model' refers to the finite element 'stick model' of the nose and main gear systems, Fig. 14, with stiffness properties used to transfer loads into the fuselage correctly. The dynamic model refers to a SIMULINK nonlinear mathematical model of the landing gear system described in this section. The landing gear mass distributions included in M05 and M14 were modified to

separate the "static mass items", e.g., braces, posts, etc., from the moving mass items, e.g., tires, wheels and shock struts. Table 3 lists the weights of the main components of the nose and main landing gears for the Boeing HSCT 1080-892STR E model. Forty percent of the total weight of the nose gear, 821.1 lbf, corresponds to moving mass and fifty-five percent of the total weight of one main gear, 4352 lbf, corresponds to moving mass. The moving mass was taken out of the M05 and M14 mass distributions used for FEM eigenvalue calculations, and then included in the SIMULINK airframe/landing gear model for transient response calculations.

The nose and main landing gear dynamics models consist of a simple mass-spring-damper system excited by the ground-induced motion of the support point as shown Fig. 15. Nonlinear spring and damping gear forces are modeled as a function of stroke using the empirical curves shown in Figures 16 and 17. Data points used as a basis for the faired curves are denoted by open circles. Stiction and friction forces in the oleo strut mechanism have been neglected. The moving mass of the gear is represented by a lumped mass and a nonlinear spring in contact with the ground represents tire stiffness. Tires are represented having a single point of contact with the ground, therefore no tire footprint information is used. The tire model for the main gear is based on the load-deflection characteristics of the Michelin 50X20-20 radial belted main-gear tire for the Boeing 777 transport aircraft. Nose gear tire stiffness characteristics are based on H37X14-15 tires. Figure 18 shows the load versus deflection curves for the nose and main gear tires. These curves represent the sum of parallel springs, 2 springs for two nose gear tires, and six springs to represent the six tires on each main gear. The damping characteristics of the tires were not available.

4.1 Runway Model

Figure 19 shows the elevation-versus-distance profile for a 3100 ft runway section in San Francisco which is commonly used by the FAA for airplane certification. The runway elevation is measured with respect to sea level. A 10,000 ft long runway profile is constructed for the simulations by appending the 3100 ft runway section every 3100 ft resulting in a periodic profile. This runway profile is the only one used in this investigation. HSCT runway x-coordinate time histories (runway x-coordinate defined along the length of the runway) in conjunction with the 10,000 ft San Francisco runway profile are used to generate elevation-versus-time histories for various ground operations. As an example, runway x-coordinate time histories for a rejected takeoff (RTO) simulation

are shown at the top of Fig. 20 with the resulting RTO runway elevation time history at the bottom.

5. System Integration / Numerical Simulations

SIMULINK, a computer simulation program, was used to combine and integrate the airframe/landing gear systems described in the previous sections. The system dynamics described in Eqs (3-5) are represented in SIMULINK blocks depicted in Figure 21. Blocks labeled "nose" and "main" contain tabulated information for the nonlinear response of the main and nose landing gears. Displacements and velocities of the airframe at the gear locations and the runway elevations are input to these blocks and gear forces are output from the blocks. These gear forces are then input into the block labeled "State-Space" and airframe displacements and velocities are the output. The SIMULINK diagram shows the interconnection between the different systems. The additional blocks shown are for decomposing vectors (Demux- turns vectors into scalar quantities) or assembling (Mux) vectors.

Since the equations of motions are nonlinear, the first step in the solution process is to determine the equilibrium states. Equilibrium states are computed when the rate of change of system states are zero after all forces have been applied. Initially, the airframe weight is applied to the landing gear producing an equilibrium state in which the landing gears are compressed. All further simulation results are generated about this equilibrium state. Aircraft responses are displayed at thirteen locations on the aircraft as indicated in Fig 22.

6. Simulation Results

6.1 Aircraft response during ground operations

The mathematical model described above has been used to simulate the HSCT response during ground operations on a San Francisco runway. Ground operations simulated are taxiing, rejected takeoff, and landing. Aerodynamic lift forces have been neglected for all cases.

6.2 Taxiing simulations

Taxiing simulations were conducted for a forward speed of 44 ft/sec (30 knots). Figures 23 and 24 show the vertical and angular response at the cockpit location for a time interval of 80 seconds. Peak half-amplitude vertical displacements at the cockpit with respect to the runway profile range from 0 to 3.5 inches with peak accelerations ranging from 0 to 0.38 g's. Pitch angular displacements of ±0.24 degrees are also observed at the cockpit location. The rigid-body heave and pitching motions as well as contributions from higher frequency modes can easily be seen on the time histories. Figures 25 and 26 show the maximum vertical displacements, normalized with respect to the runway profile, and accelerations at the 13 sensor locations on the airframe. Although the maximum displacement and acceleration on the fuselage occur at the cockpit location, the displacement and acceleration at the mid and aft sections of the fuselage also show considerable response.

6.3 Rejected Takeoff simulations

A rejected takeoff (RTO) scenario was chosen over a normal takeoff because it is considered the worse-case scenario in terms of pilot workload. For the RTO simulation the aircraft accelerates from 0 to a maximum of 170 knots in 35 seconds, an engine failure or some other aircraft malfunction then causes the pilot to abort the takeoff and decelerate to zero speed in 20 sec. The forward speed profile used for the RTO simulation is shown in Fig. 27. For the given runway elevation profile aircraft responses have been computed at all sensor locations described previously. Response time histories at the cockpit location are presented in Figures 28 and 29. Vertical displacements at the cockpit reached a maximum of 6.5 inches (half-amplitude relative to the runway profile) with peak accelerations of 1.4 g's. Pitch angular displacements of ±0.35 degrees are obtained at the cockpit with angular accelerations ranging from 0 to 70 deg/sec^2. Again, the participation of the rigid-body heave and pitch modes and flexible modes to the total response is evident in the time histories. Maximum displacements and accelerations over the airframe, Fig. 30-31, are all of considerable magnitude. Maximum response occurs at the wing tip (location 11).

A separate RTO simulation using only rigid-body modes of the airframe was conducted to assess the contribution of the rigid body modes to the total response. Results showed that

60 to 70% of the total response is due to rigid-body motion and 30 to 40% is due to the elastic response of the airframe.

6.4 Landing simulations

Landing simulations of the HSCT were conducted at a landing weight condition of 388,584 lbf, mass case M14, for a time interval of 20 sec after nose gear touch down. The forward speed profile for the simulation is shown in Fig 32. The simulation starts with the aircraft on the ground at a maximum forward speed of 120 knots and continues with the aircraft decelerating to a complete stop. Aerodynamic lift effects are neglected. Results are summarized in Figures 33 through 36. Heave and pitch motions are dominated by the low-frequency aircraft modes, with maximum vertical displacements relative to the runway of 4.3 inches and a maximum rotation of +0.25 degrees. Peak acceleration at the cockpit reached a maximum of 1.2 g's. Again, displacements and accelerations at other locations on the airframe are all of considerable magnitude but in this case the cockpit had the highest values.

6.5 Frequency Comparison of the Various Ground Operations

The Power Spectral Density function (PSD) was computed from the acceleration time history at the cockpit location and RMS values calculated at various frequency bandwidth intervals in the frequency range from 0 to 22.6 Hz. Figure 37 shows a summary of the cockpit squared RMS acceleration for all three ground operations. Based on the squared RMS one can estimate the RMS responses at a given frequency by computing the square root of the plotted value. During taxiing the rigid body vertical and pitching motions and the first two flexible symmetric and antisymmetric airframe modes are the largest contributors to the RMS response. Cockpit acceleration levels for the RTO case show RMS acceleration levels in excess of 0.28 g's around 2 Hz which coincide with some of the airframe flexible modes. The contribution of the rigid and flexible modes in the frequency range of 0.7071 to 1.4104 is also noticeable. Cockpit acceleration levels for the landing case showed RMS acceleration levels of about 0.14 g's around 2 Hz.

6.6 Human Response to Vibration

The results of some early studies on human tolerance to vibrations which were presented in Ref. [12] are reproduced here in Figure 38. Note that levels of 0.5 g's are considered intolerable in the low-frequency range between 1 and 5 Hz. The HSCT acceleration levels at the cockpit during taxiing, RTO, and landing discussed in the previous sections are all within the intolerable range. Pilot-in-the-loop simulator studies made by the Boeing Co. have shown that vibration amplitudes exceeding 2 inches at low frequencies are considered unacceptable. A need for active vibration suppression is evident based on this results.

7. Concluding Remarks

Numerical simulation of the Boeing High Speed Civil Transport 1080-920STR Model E configuration during taxiing, take-off, and landing operations have been presented. Linear finite element models of the airframe are used and combined with nonlinear landing gear models to provide a simulation model which is used to examine dynamic response to ground input conditions. A commercial computer simulation program was used to numerically integrate the equations.

Simulation results showed vertical displacements and RMS acceleration levels at the cockpit location and passenger cabin exceeding safe acceptable human response levels. Since the aircraft response is dominated by the heave and pitch rigid-body modes and the first low-frequency flexible modes, some type of actively or semi-actively controlled landing gear should be employed to improve the ride quality of the aircraft during ground operations, Ref. [11].

8. References

1-Mitchell, C.G.B., Some Measured and Calculated Effects of Runway Unevenness on a Supersonic Transport Aircraft. Symposium on Nonlinear Dynamics, Loughborough University of Technology, March 1972.

2- Irwin, K.S. and Andrews, W.H., Summary of XB-70 Airplane Cockpit Environmental Data. NASA TN D-5449, October, 1969.

3- Shepherd, A., Catt, T. and Cowling, D., The Simulation of Aircraft Landing Gear Dynamics. International Council of the Aeronautical Sciences, Beijing, People's Republic of China, pp. 21-25 September, 1992.

4- Doyle, G.R. Jr., A Review of Computer Simulations for Aircraft -Surface Dynamics, J. Aircraft, Vol. 23, No. 4, April 1986.

5- SIMULINK User's Guide, August 1995 Revision, The MathWorks Inc., Natick, Mass.

6- Dawdy, J. R., Dornfeld, G.M., Phillips, B.A., High Speed Civil Transport Reference H-Cycle 1 Simulation Database, NASA Contract NAS1-19360, Task Assignment No. 49.

7- ELFINI Basic User Guide, Vertsion 6.4, Avions Marcel Dassault-Brequet Aviation, June 1990.

8- MSC/NASTRAN Basic Dynamic Analysis User's Guide,V68, First printing December 1993, The MacNeal-Schwendler Corporation, Los Angeles, California.

9- Hurty W.C. and Rubinstein, M.F., Dynamics of Structures, 2nd Edition, Prentice Hall, Inc., Englewood Cliffs, N.J.

10- Mitchell, P.M., Advance Finite Element Weight Estimation Process on the High Speed Civil Transport. Society of Allied Weight Engineers, Inc. . SAWE Paper No.2169. Category No. 23. May 1993.

11- Catt, T., Cowling, D. and Shepherd, A., Active Landing Gear Control for Improved Ride Quality During Aircraft Ground Roll. AGARD Specialists Meeting on Smart Structures for Aircraft and Spacecraft , AGARD CP531, Lindau Germany, 1992.

12- Goldman, D.E., and von Gierke, H.E., Effects of Shock and Vibration on Man, Shock and Vibration Handbook, Vol. 3, Chapter 44, 1961.

Table 1. HSCT model sections and offsets

Boeing Num.	Section Description	Section ID	Base Node	Base Elem	Base Prop	Base Mat.
E14	nosecone	nc	0	0	0	0
E03	fwd body	fb	1000	1000	100	100
E04	mid body	mb	5000	5000	200	200
E05	aft body	ab	10000	10000	300	300
E06	vertical tail	vt	15000	15000	400	400
E07	horizontal tail	ht	16000	16000	500	500
E12	rudder	rud	17000	17000	600	600
E13	elevator	el	18000	18000	700	700
E08	inboard eng	ie	20000	20000	800	800
E09	outboard eng	oe	22000	22000	900	900
E01	inboard wing	iw	25000	25000	1000	1000
E10	inb. controls	ic	30000	30000	1100	1100
E11	outb. controls	oc	32000	32000	1200	1200
E02	outboard wing	ow	35000	35000	1300	1300

Table 2. HSCT sample component kinetic energy summary table

Section	Mode 4 1.3 Hz	Mode 5 2.0 Hz	Mode 6 2.6 Hz	Mode 7 2.7 Hz	Mode 8 3.1 Hz	Mode 9 3.1 Hz
E14-nosecone	.3	0.0	0.1	0.0	0.1	0.0
E03-fwd body	50.1	1.4	6.2	0.1	5.6	2.2
E04-mid body	2.1	0.8	4.0	0.1	3.6	1.4
E05-aft body	13.2	12.6	5.6	0.1	0.3	0.1
E06-vertical tail	2.7	2.9	1.6	0.0	0.0	0.0
E07-horizontal tail	8.5	10.6	7.2	0.2	0.2	0.1
E12-rudder	0.8	0.9	0.5	0.0	0.0	0.0
E13-elevator	1.7	2.5	2.1	0.0	0.1	0.0
E08-inboard eng	1.4	2.3	9.2	97.6	4.1	1.0
E09-outboard eng	1.4	24.7	3.5	0.1	49.5	88.3
E01-inboard wing	17.3	6.9	18.4	0.6	16.5	6.3
E10-inb. controls	0.2	0.3	0.5	0.0	0.3	0.1
E11-outb. controls	0.1	7.2	9.7	0.3	4.8	0.1
E02-outboard wing	0.3	26.8	31.3	0.8	14.8	0.3
Total energy (%)	100.0	100.0	100.0	100.0	100.0	100.0

Table 3. HSCT 1080-892 Landing gear weights

Nose Landing Gear	Weight (lb/side)
Wheels	101.1
Tires	178.4
Air	7.3
Drag strut	67.2
Side strut	38.2
Shock strut	375.7
Attachment fittings	12.6
Miscellaneous	15.0
Nose gear steering	145.0
Nose gear retraction	87.5
Emergency steering	12.1
Total	1040.0

Main Landing Gear	Weight (lb/side)
Wheels	334.9
Tires	448.8
Air	22.2
Brakes	490.8
Drag struts	464.4
Side struts	73.3
Trucks	210.7
Oleos	833.1
Axles	187.6
Torsion links	105.6
Oleo fluid	50.8
Attachment fittings	286.6
Truck positioners	51.9
Miscellaneous	45.6
Retraction systems	257.1
Brake operating system	57.0
Emergency extension	19.5
Elec. operating mech.	21.9
Total	3962.0

Note : These weights are for a half-model representation of the airplane

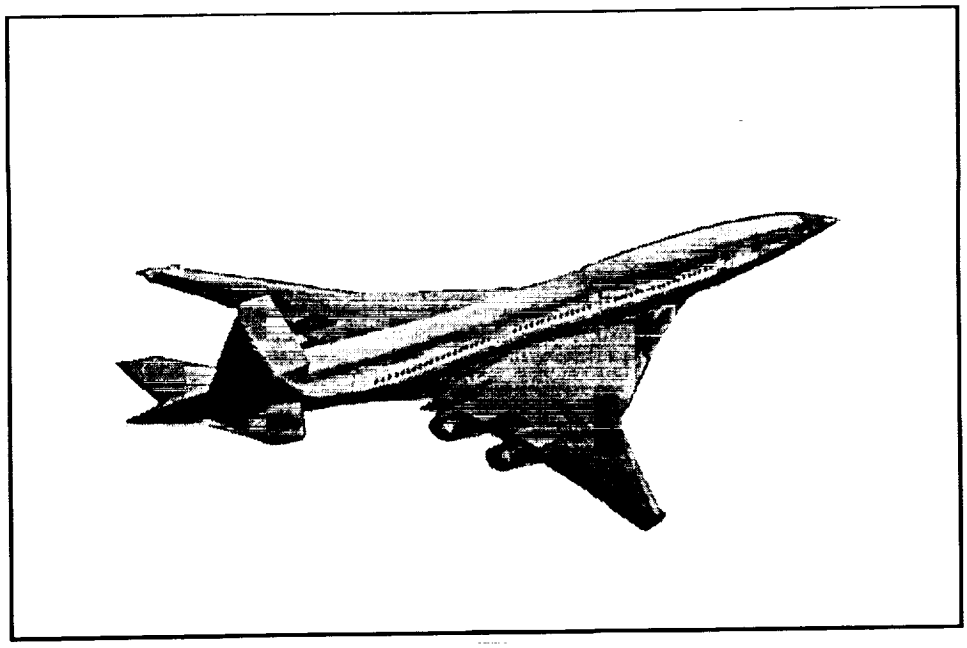

Figure 1. High Speed Civil Transport (aft tail/four engine configuration)

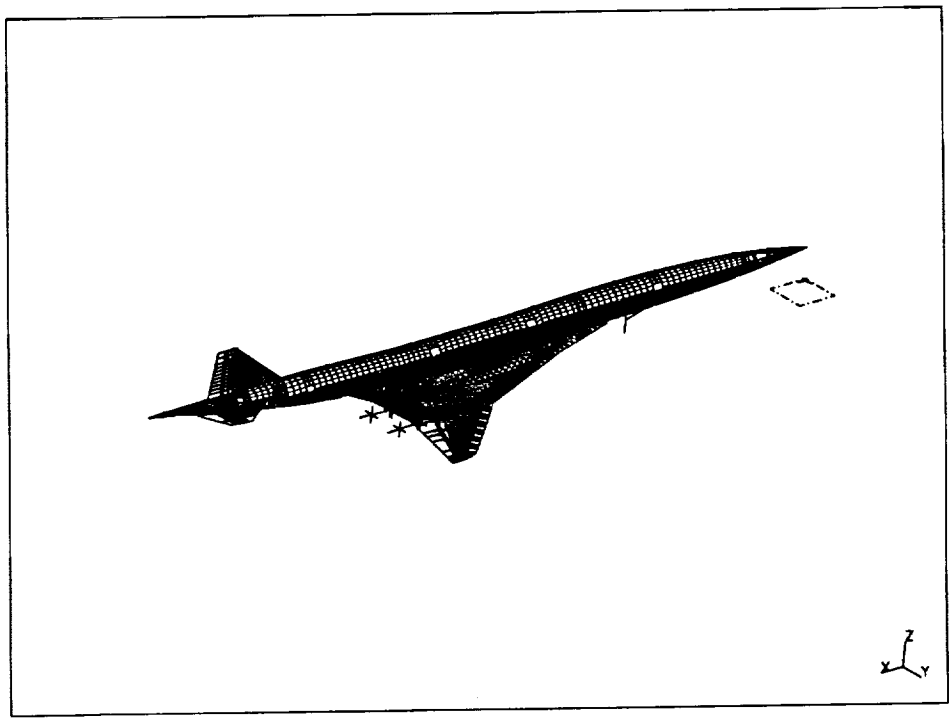

Figure 2. HSCT Finite Element (symmetrical right-half)

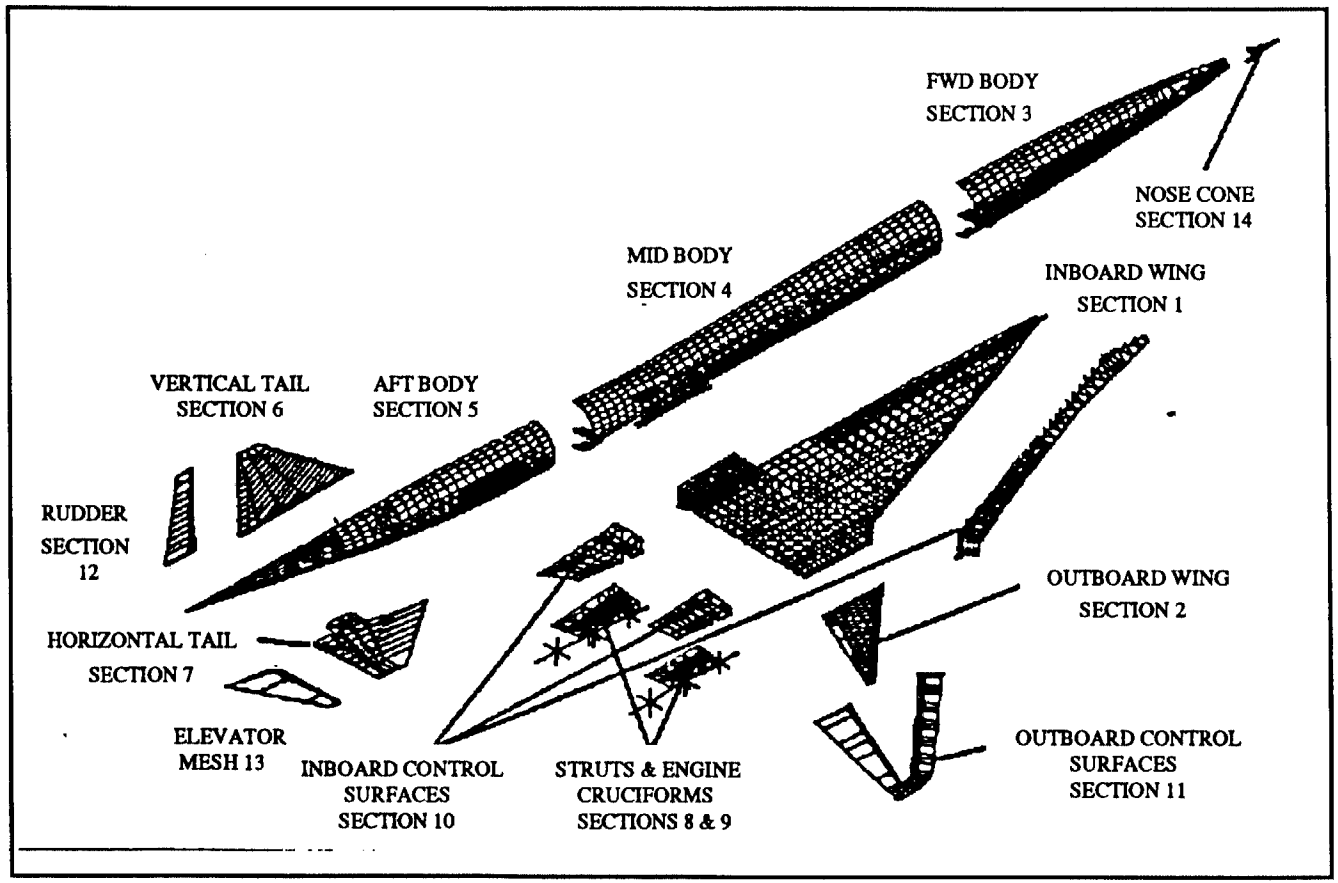

Figure 3. HSCT Finite Element sections

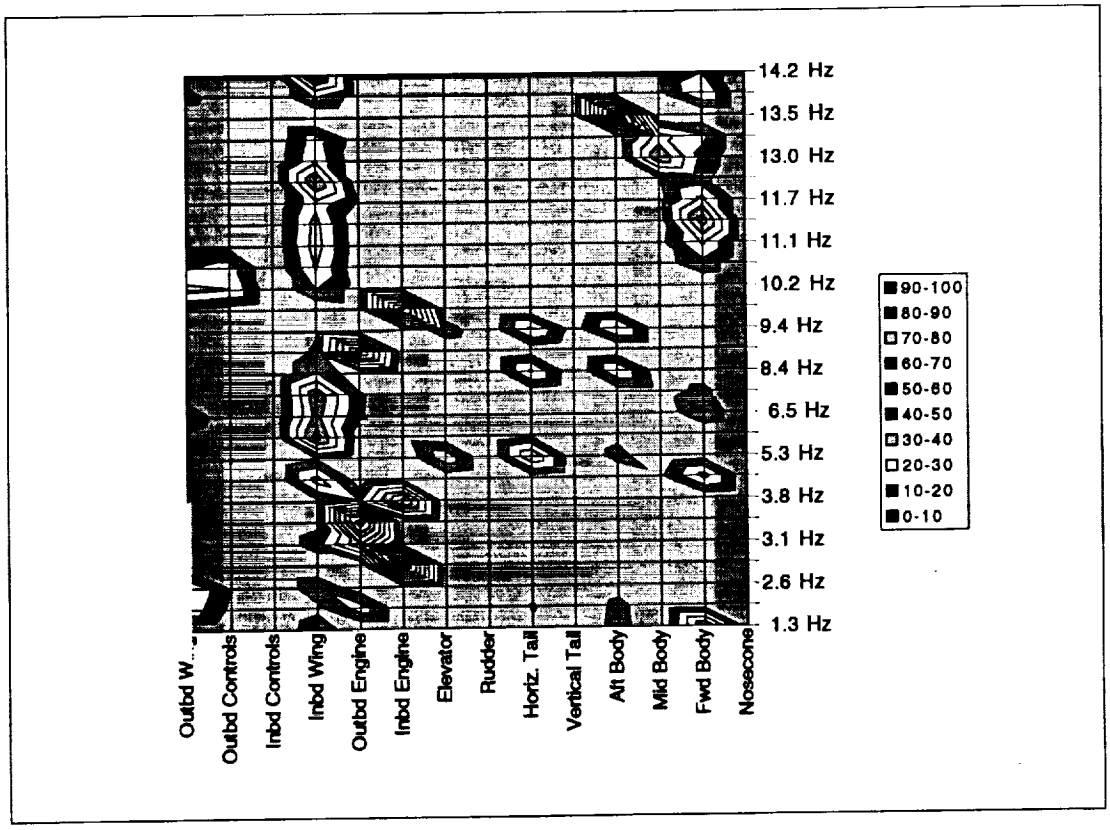

a) Symmetric boundary conditions

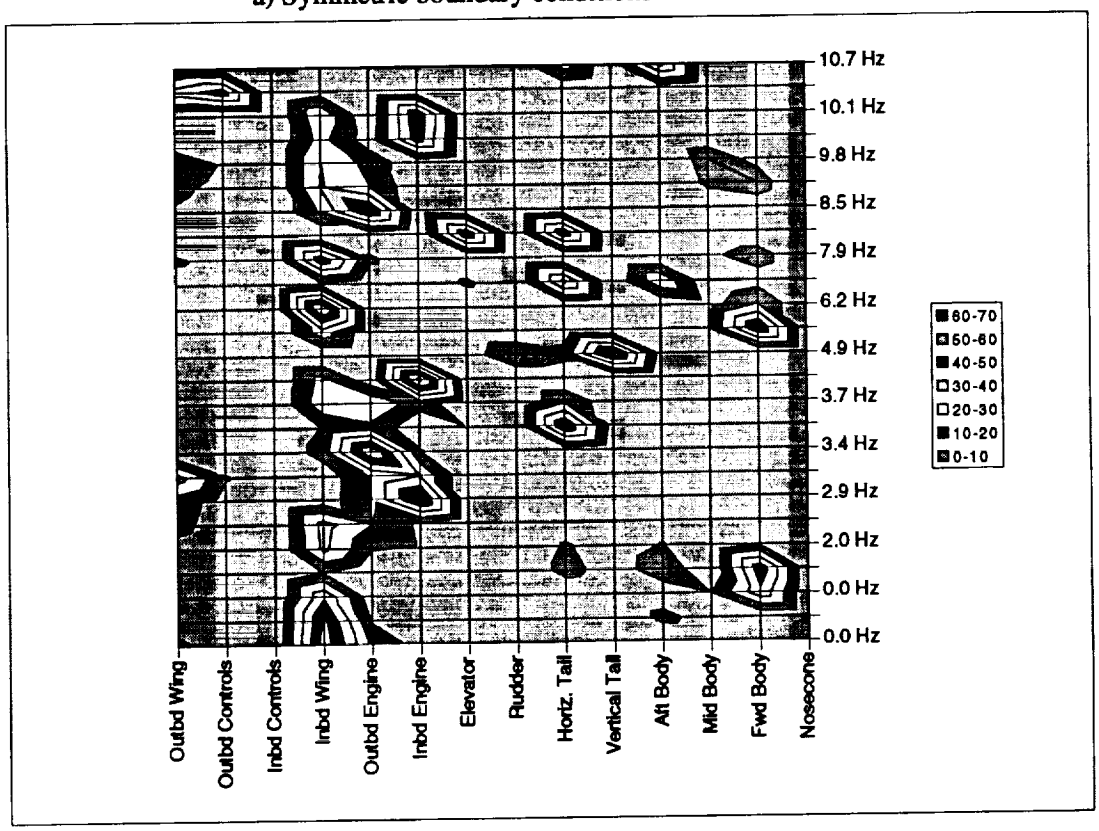

b) Antisymmetric boundary conditions

Figure 4. Modal kinetic energy data, MO5

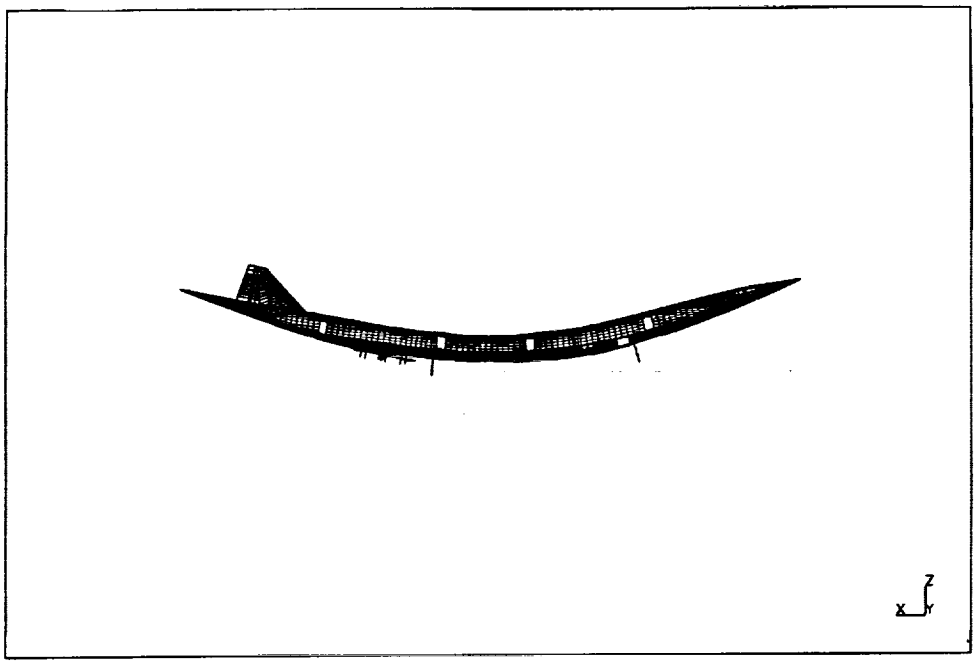

Figure 5. Mode 4, f=1.308 Hz, MO5 symmetric
f=1.2703 Hz, M14 symmetric

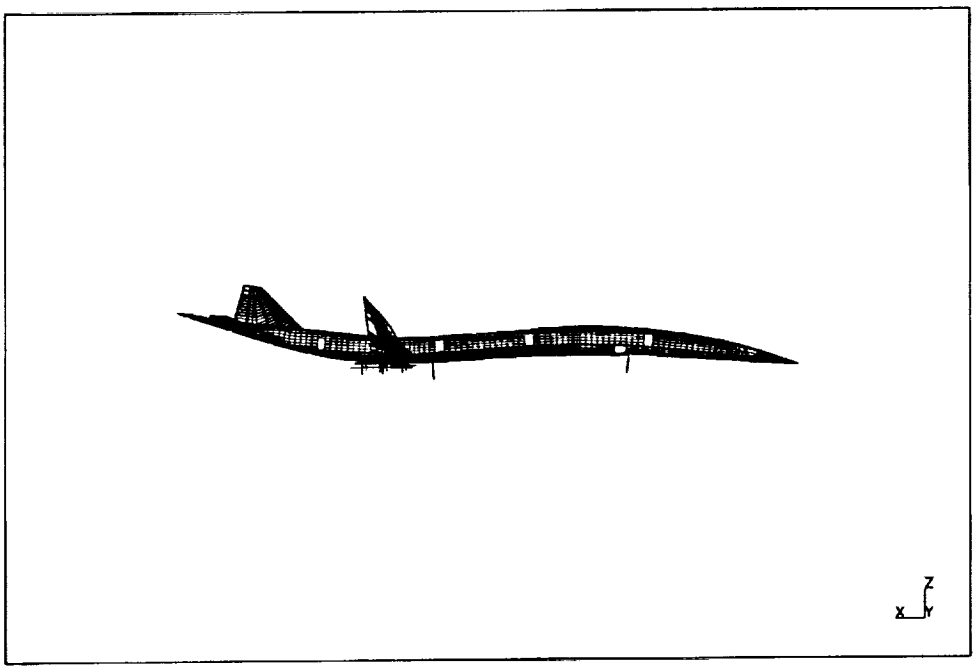

Figure 6. Mode 6, f=2.641 Hz, MO5 symmetric
f=2.6878 Hz, M14 symmetric

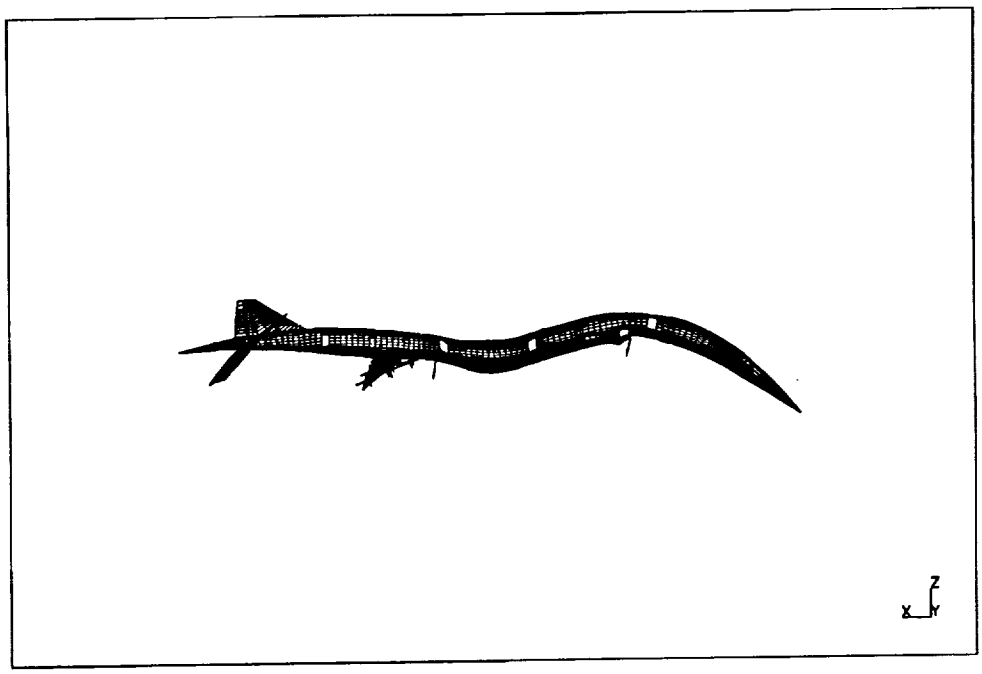

Figure 7. Mode 11, f=4.736 Hz, MO5 symmetric
f=4.721 Hz, M14 symmetric

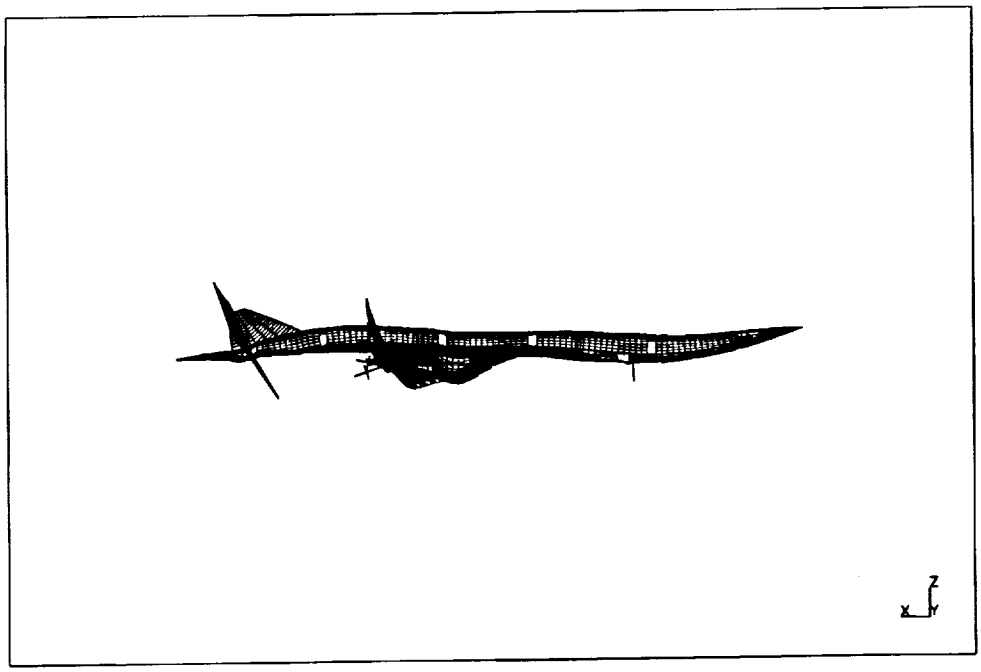

Figure 8. Mode 13, f=6.218 Hz, MO5 symmetric
f=6.674 Hz, M14 symmetric

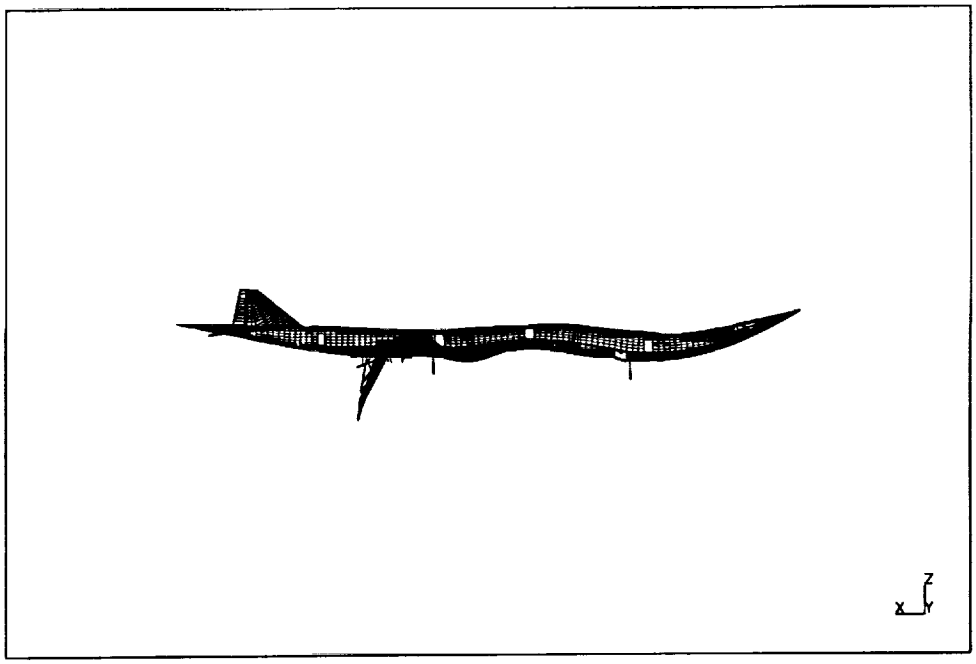

Figure 9. Mode 14, f=6.546 Hz, MO5 symmetric
no equivalent, M14

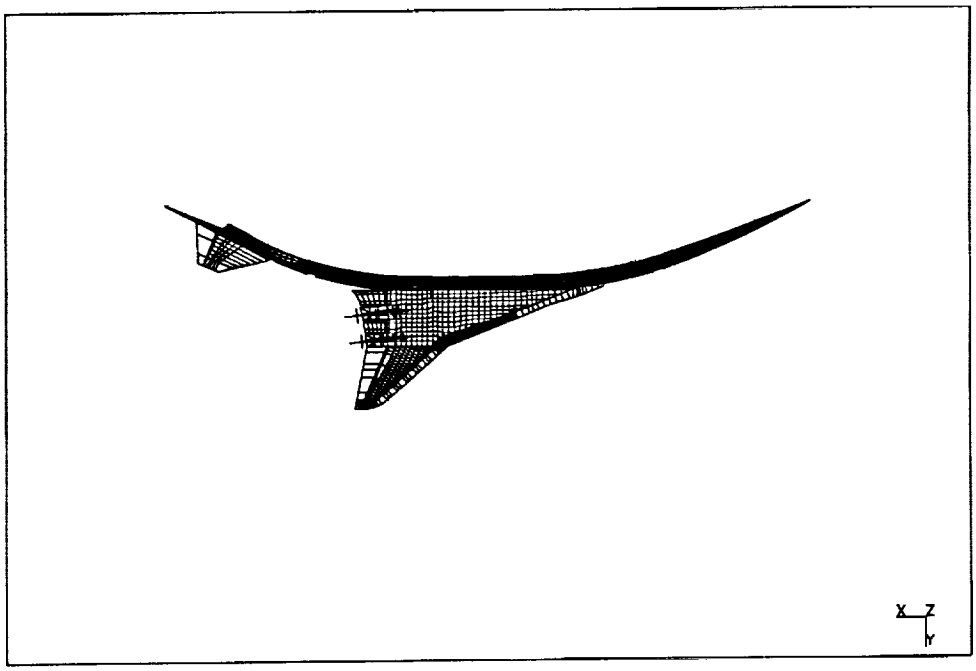

Figure 10. Mode 4, f=1.555 Hz, MO5 antisymmetric
f=1.412 Hz, M14 antisymmetric

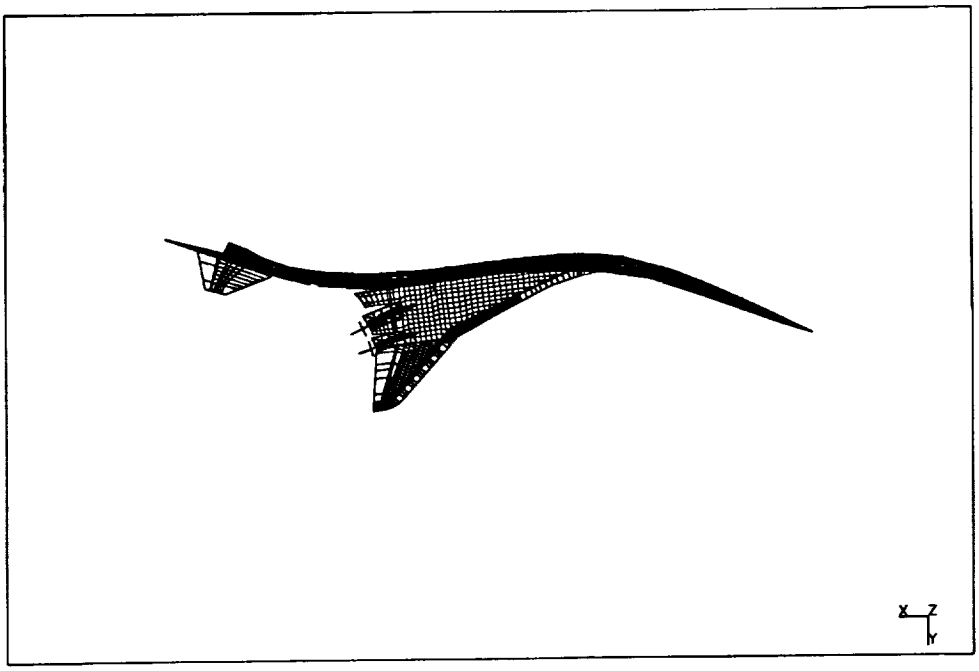

Figure 11. Mode 5, f=2.035 Hz, MO5 antisymmetric
f=2.129 Hz, M14 antisymmetric

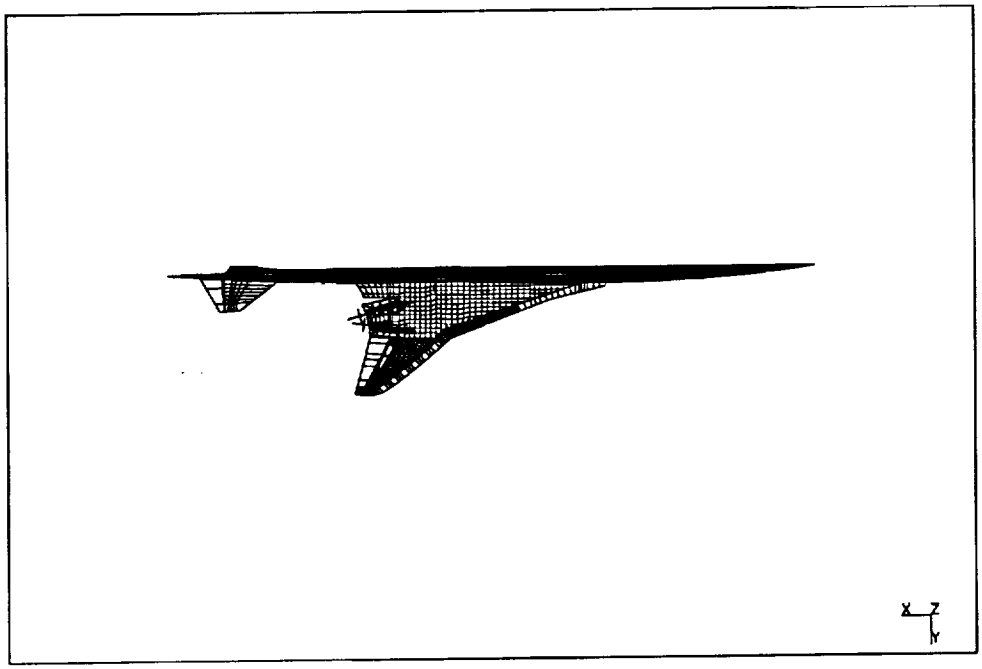

Figure 12. Mode 6, f=2.146 Hz, MO5 antisymmetric
no equivalent,M14

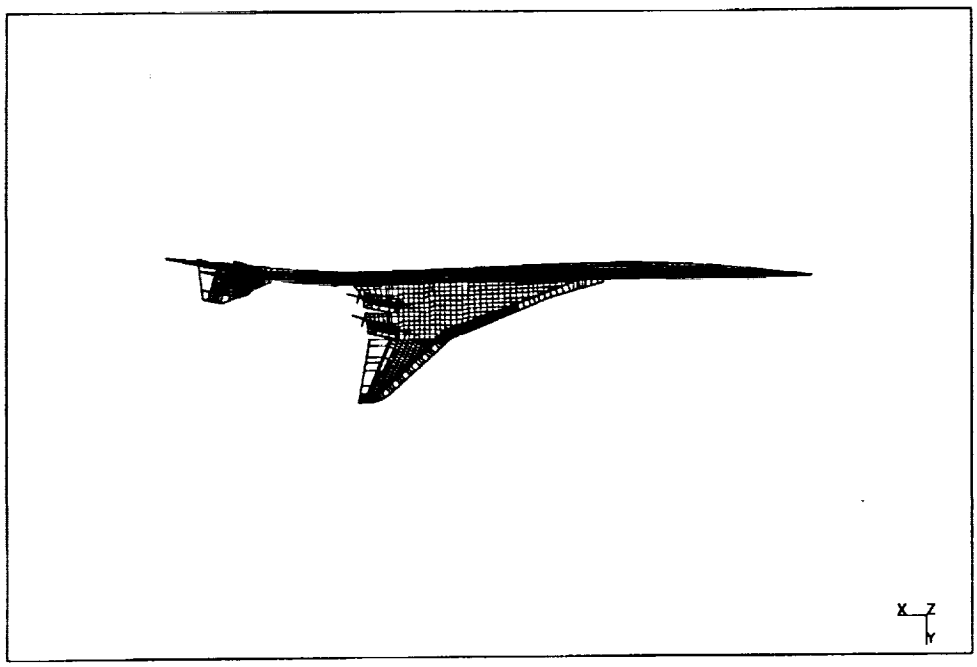

Figure 13. Mode 10, f=3.545 Hz, MO5 antisymmetric
f=3.650 Hz, M14 antisymmetric

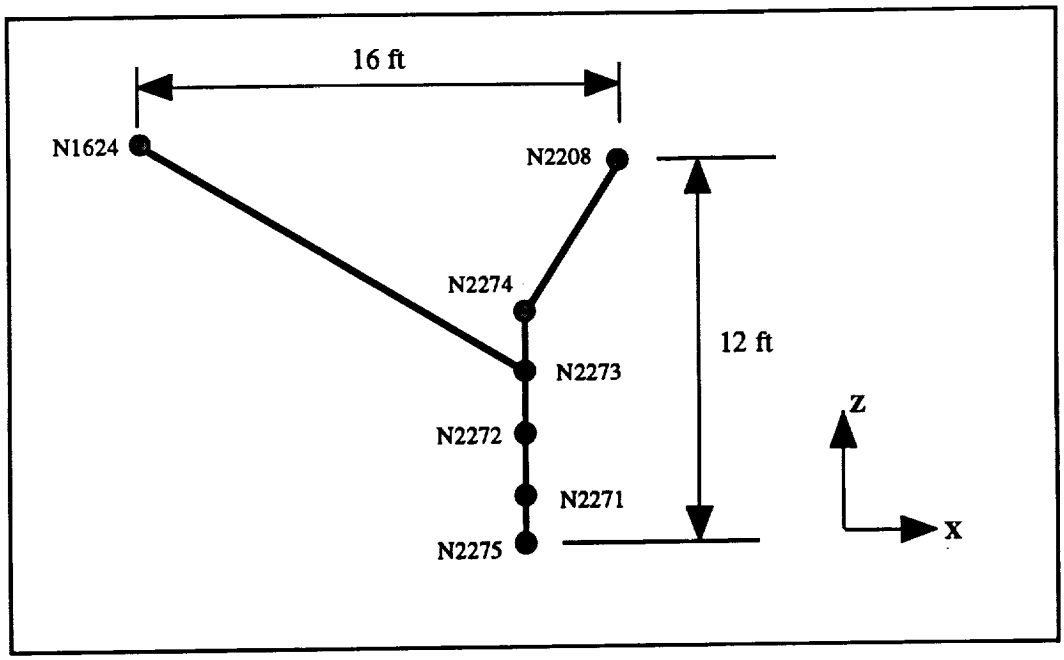

Figure 14. Nose gear structural 'stick' model

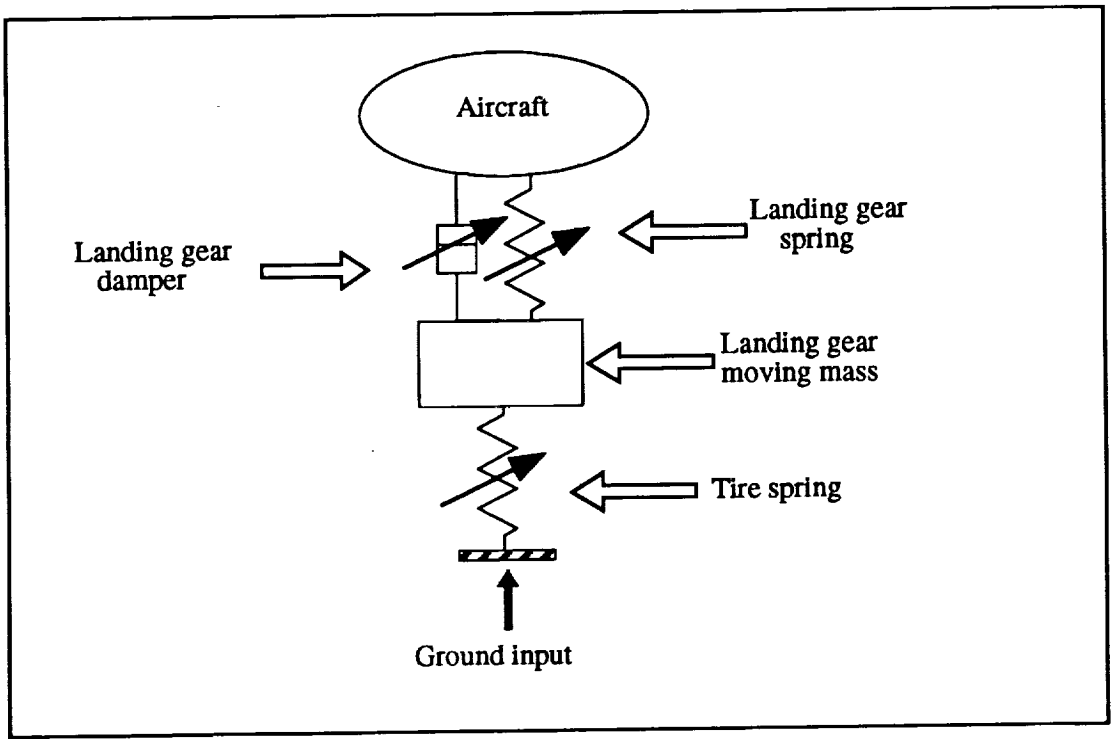

Figure 15. Landing gear dynamic model

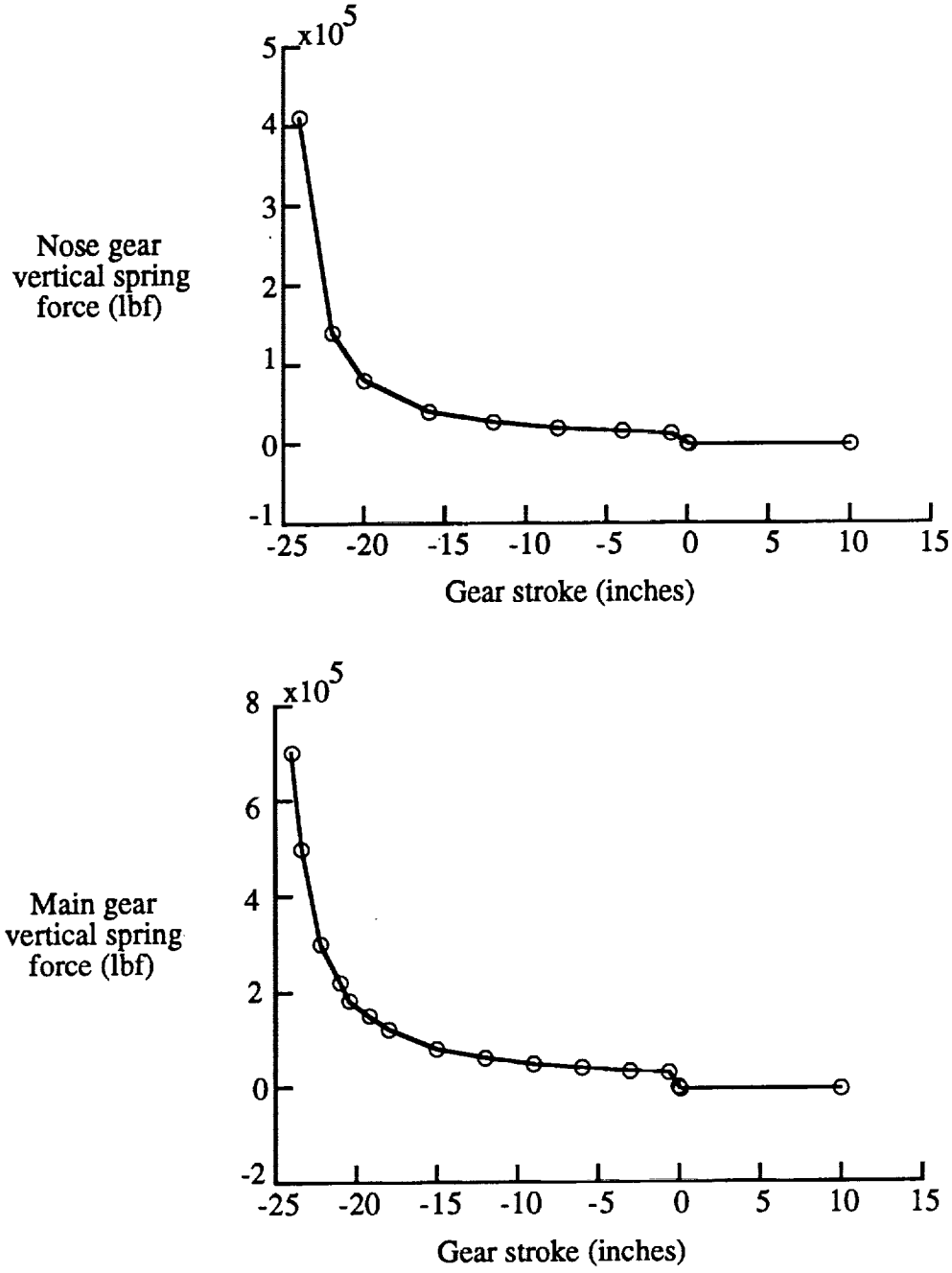

Figure 16. Nose and main gear load-stroke curves

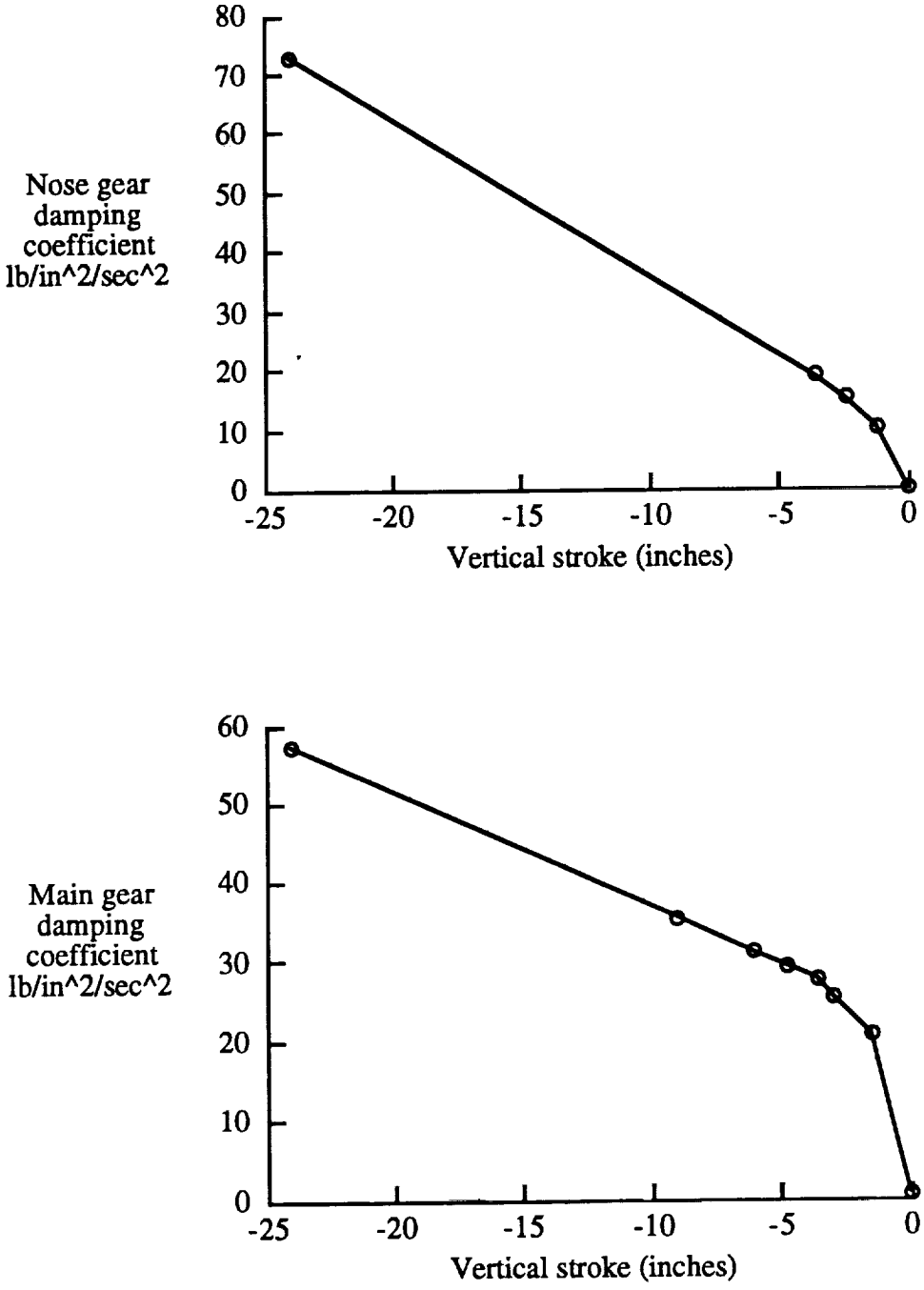

Figure 17. Nose and Main gear damping force coefficient curves

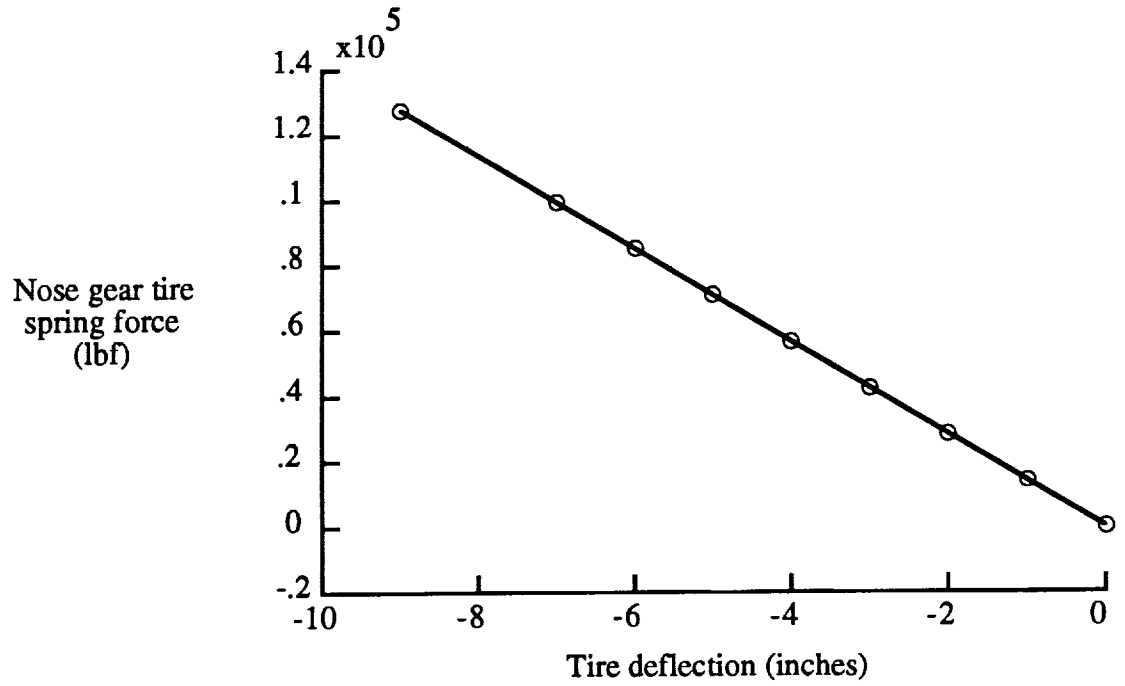

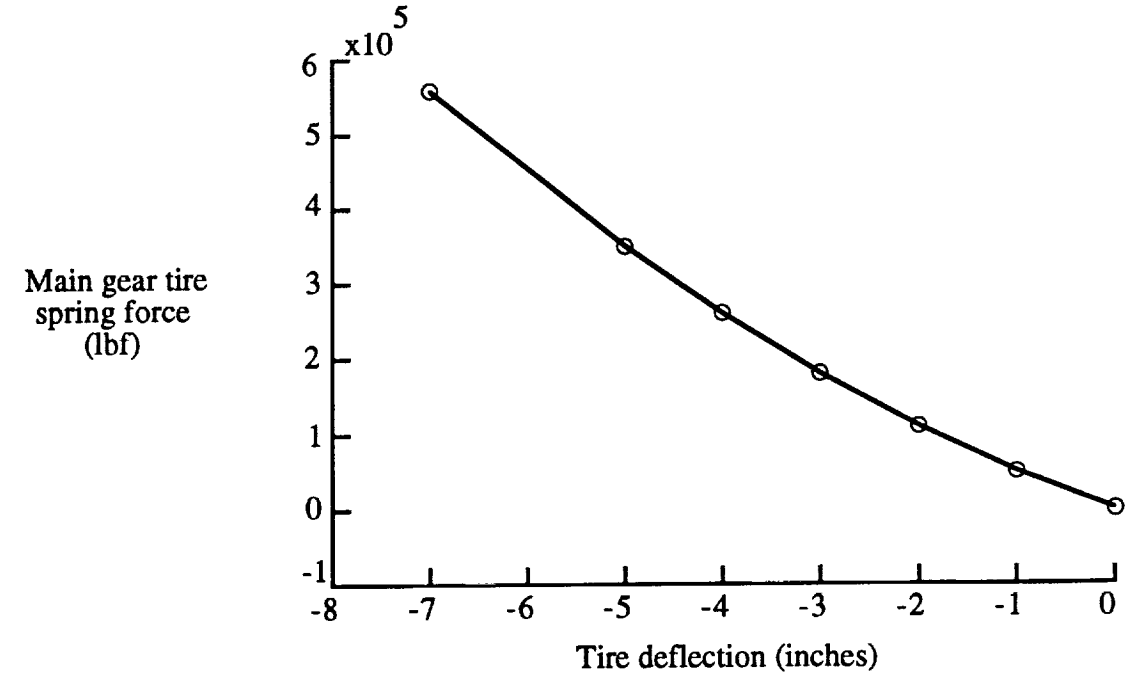

Figure 18. Nose and main gear tires spring curves

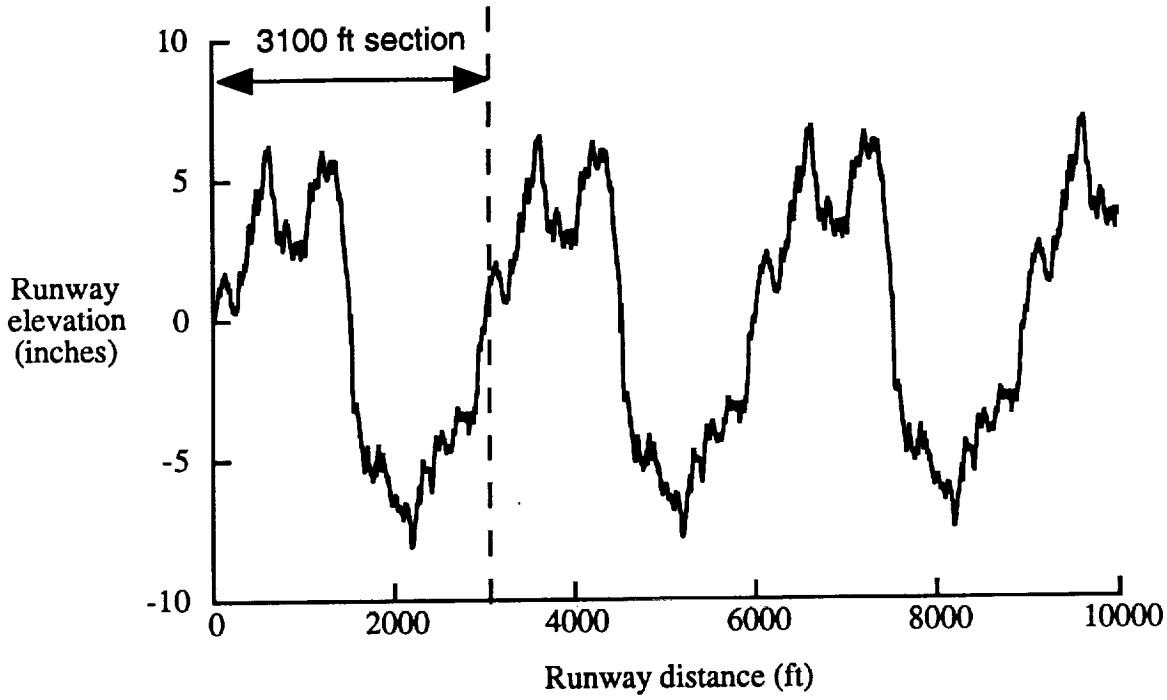

Figure 19. San Francisco runway elevation with respect to sea level profile

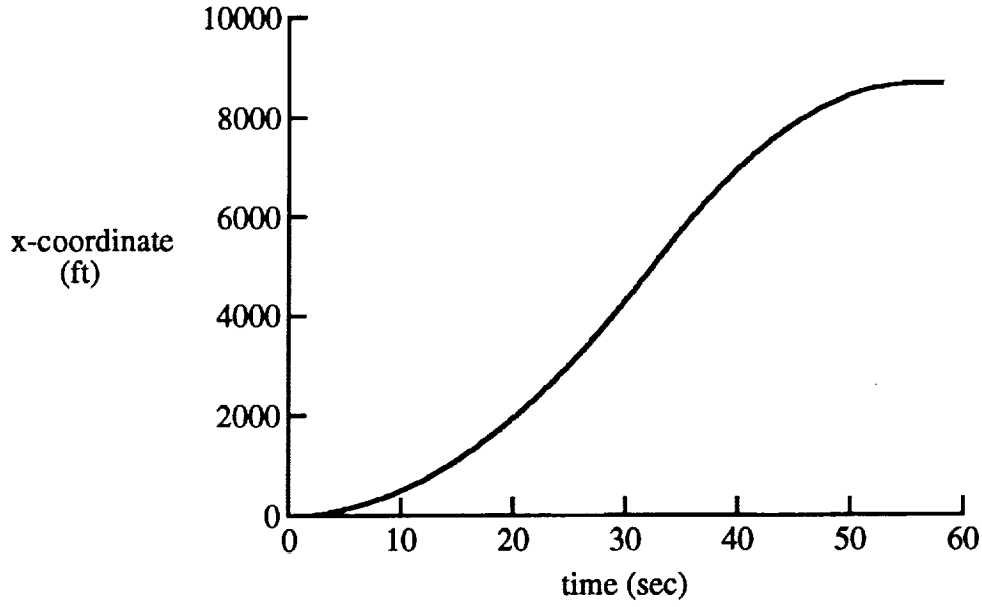

RTO runway x-coordinate time history

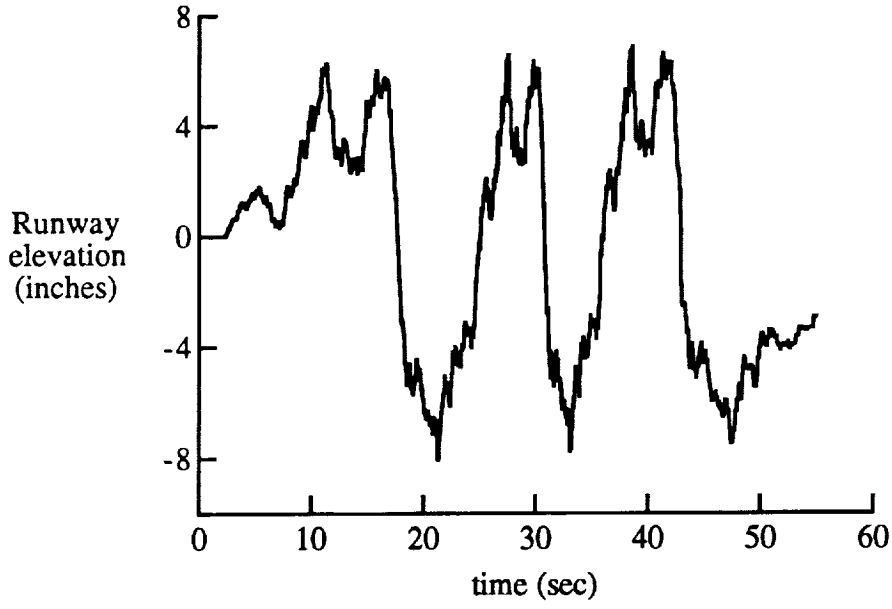

RTO runway elevation time history

Figure 20. Rejected takeoff time histories

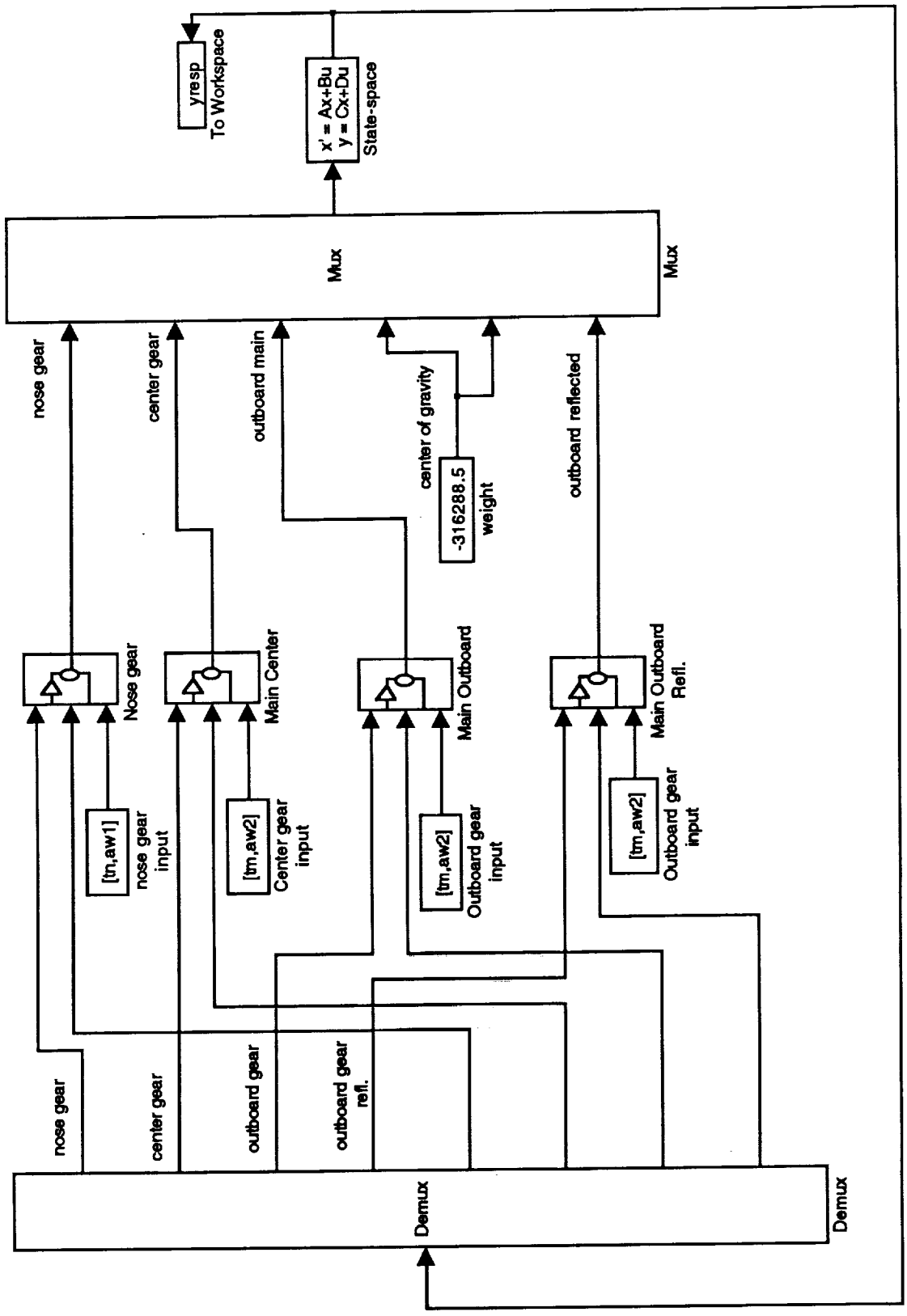

Figure 21. SIMULINK block diagram - HSCT nonlinear ground operations simulation

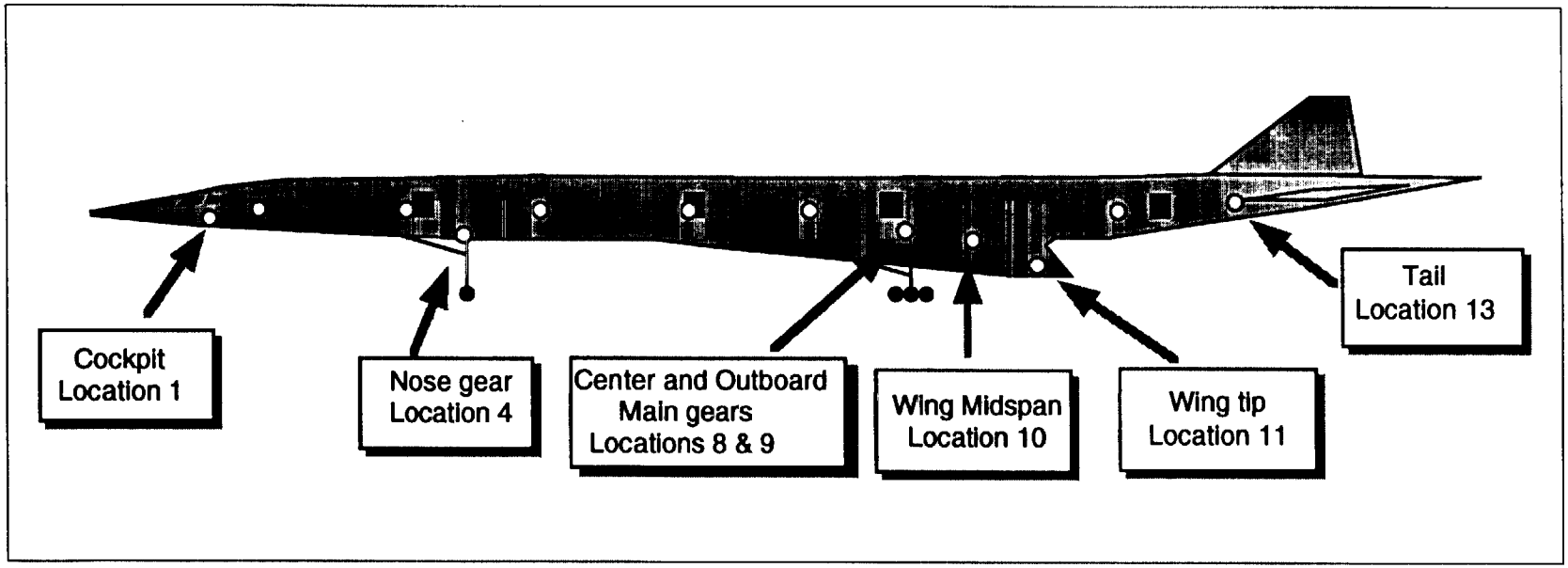

Figure 22. Sensor locations

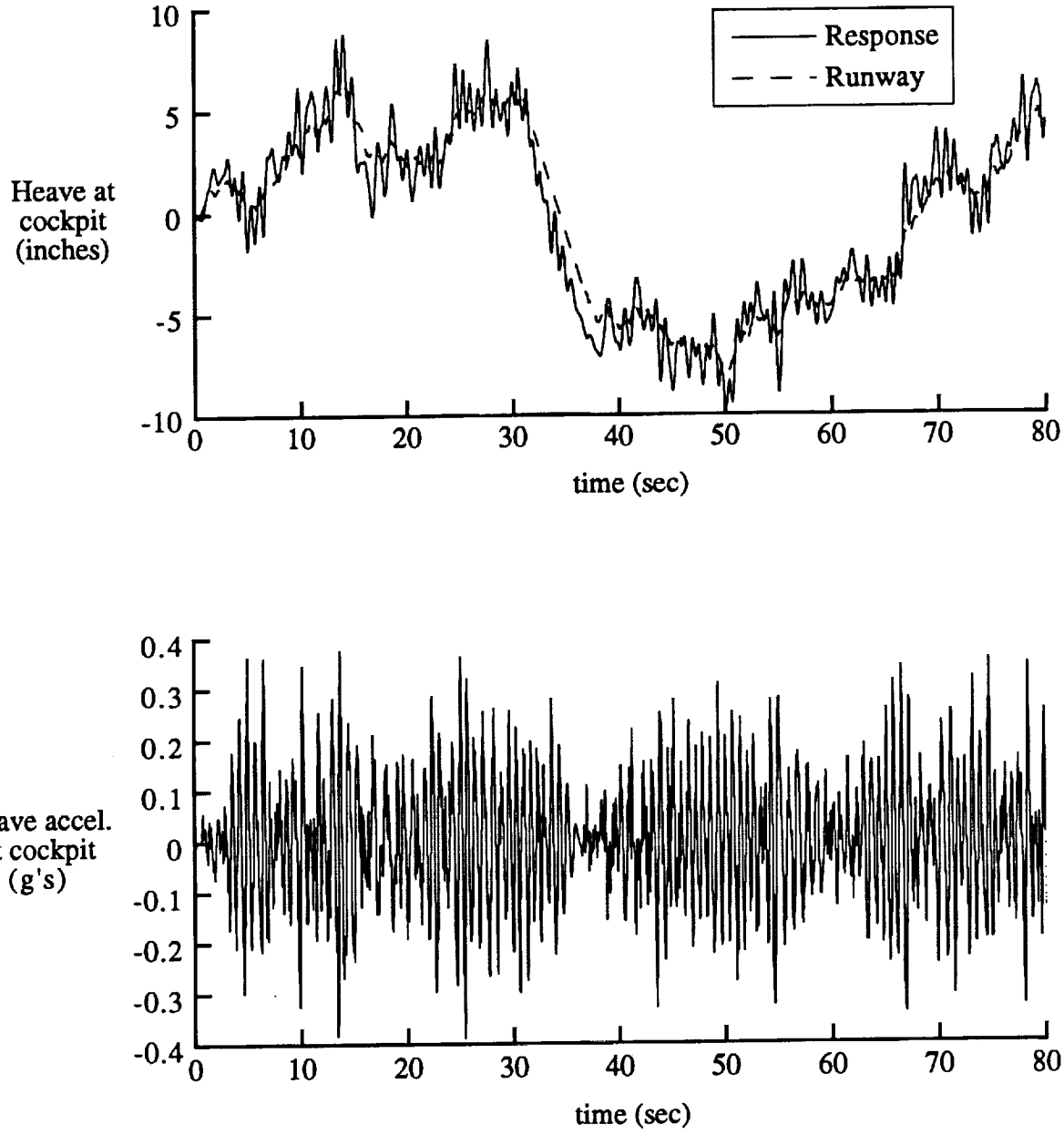

Figure 23. Taxiing vertical response at cockpit location

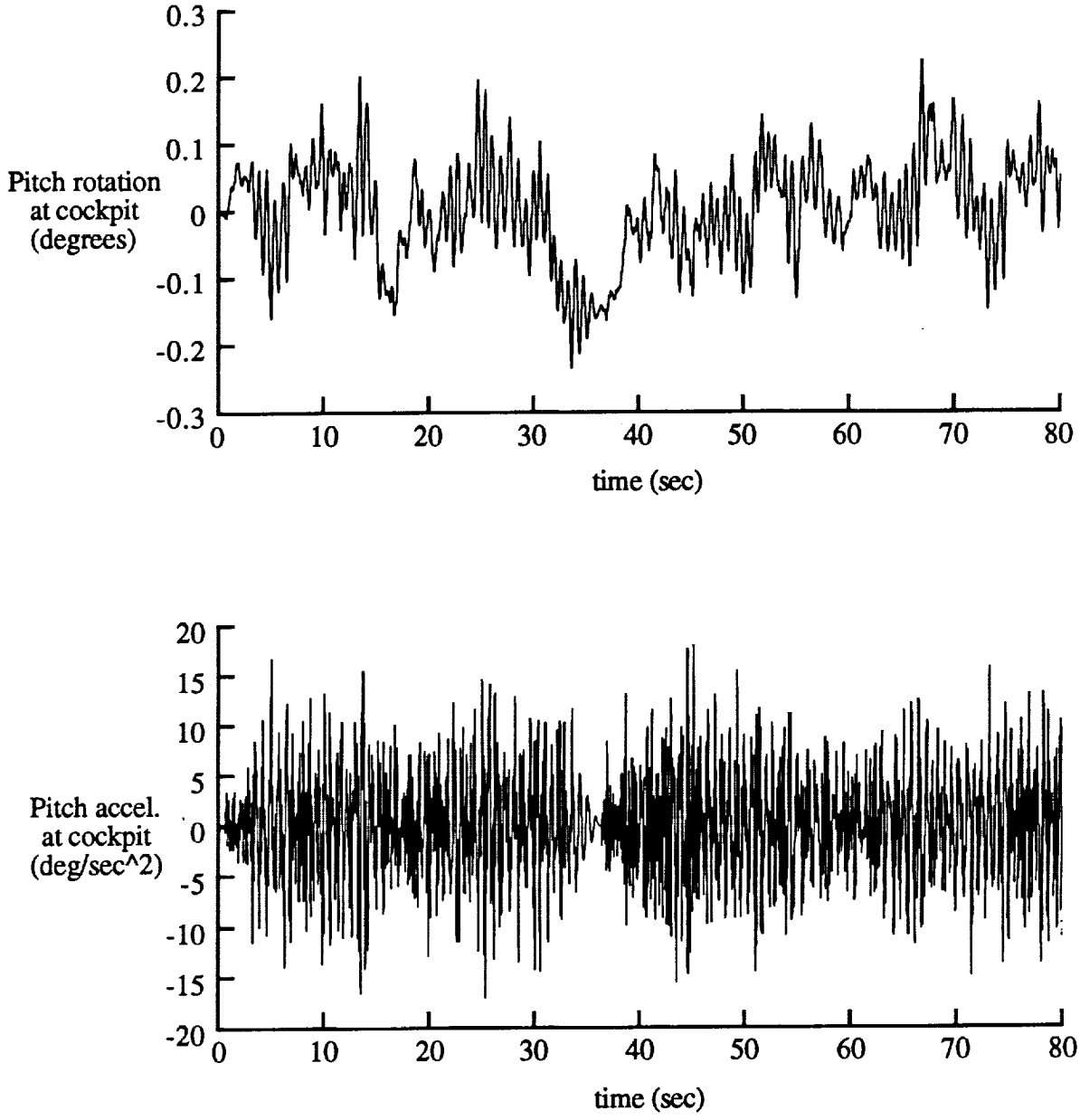

Figure 24. Taxiing pitch response at cockpit location

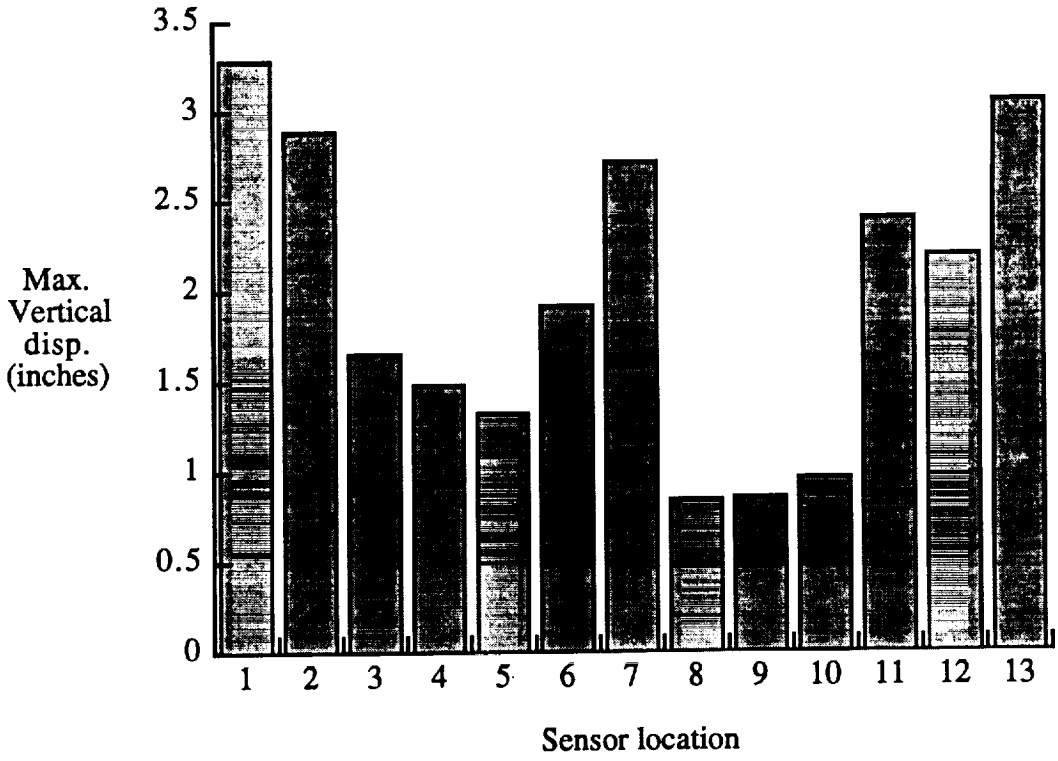

Figure 25. Taxiing maximum vertical displacements at 13 sensor locations

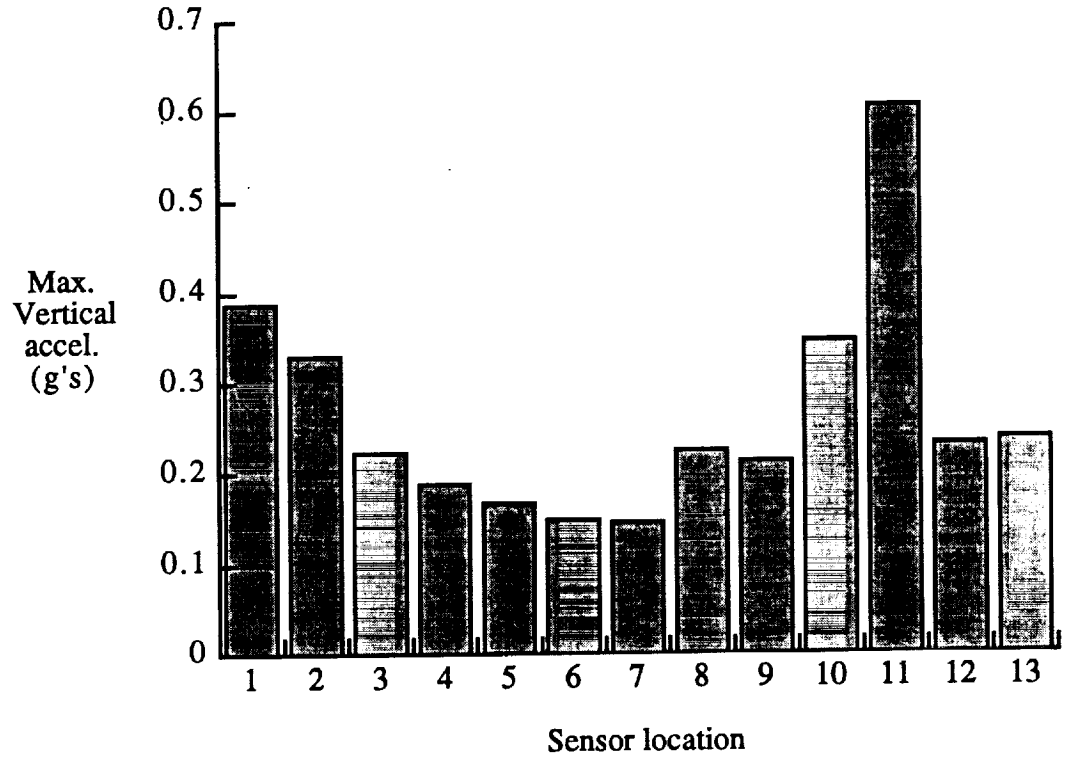

Figure 26. Taxiing maximum vertical accelerations at 13 sensor locations

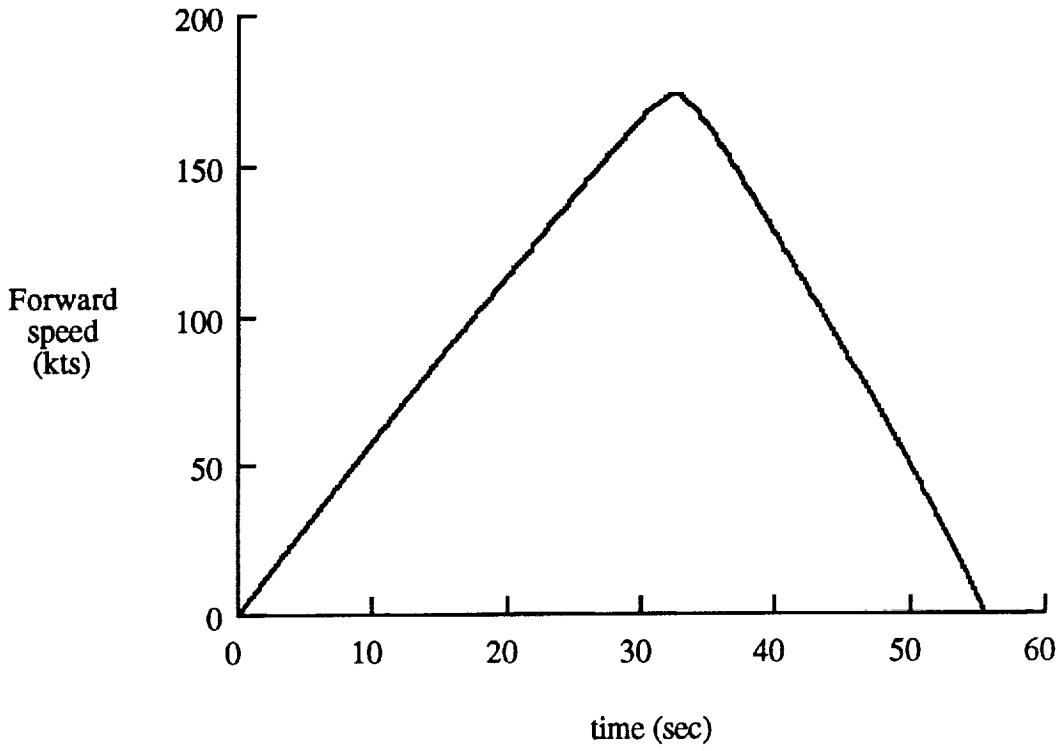

Figure 27. RTO forward speed profile

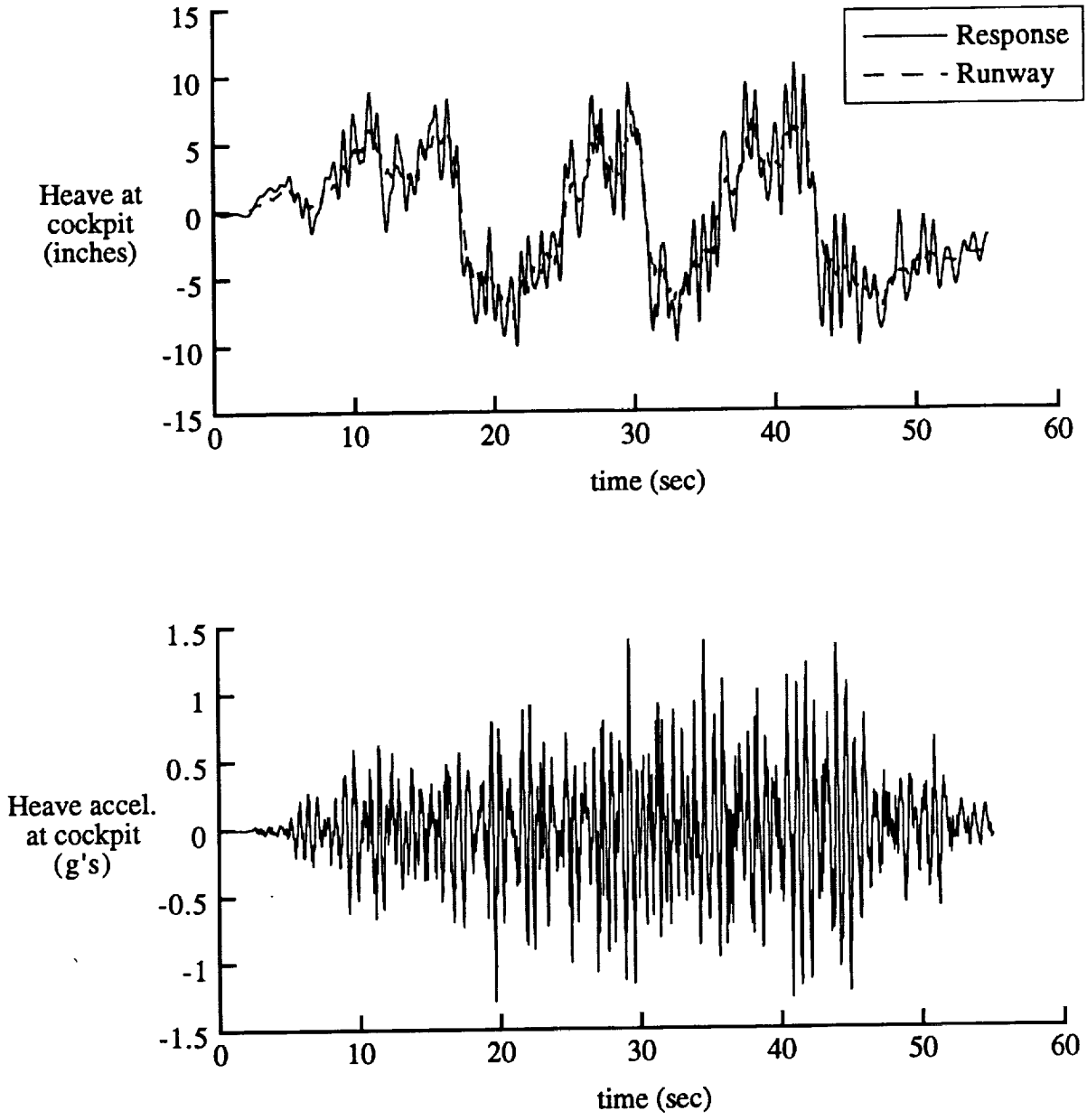

Figure 28. RTO vertical response at cockpit location

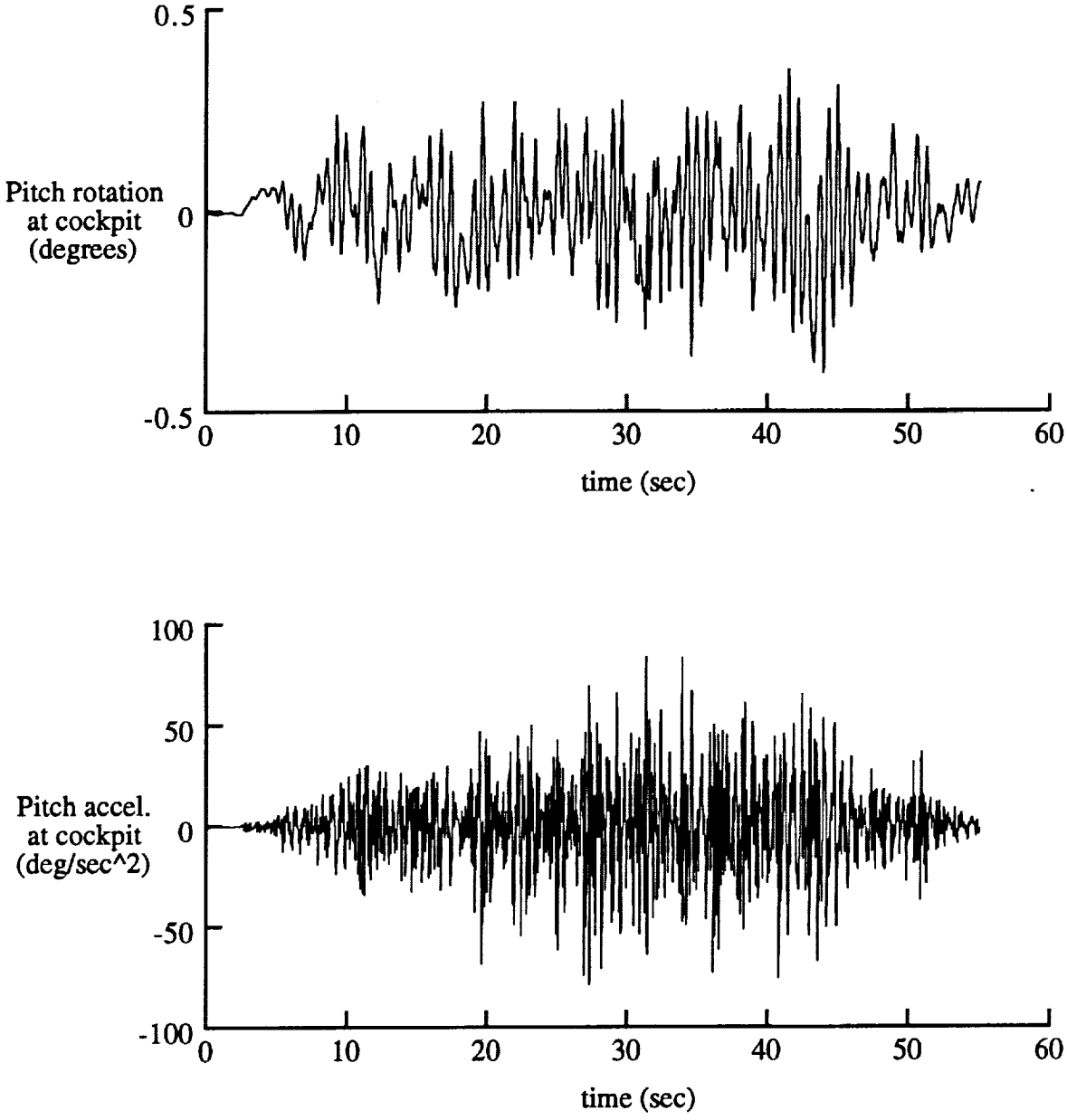

Figure 29. RTO pitch response at cockpit location

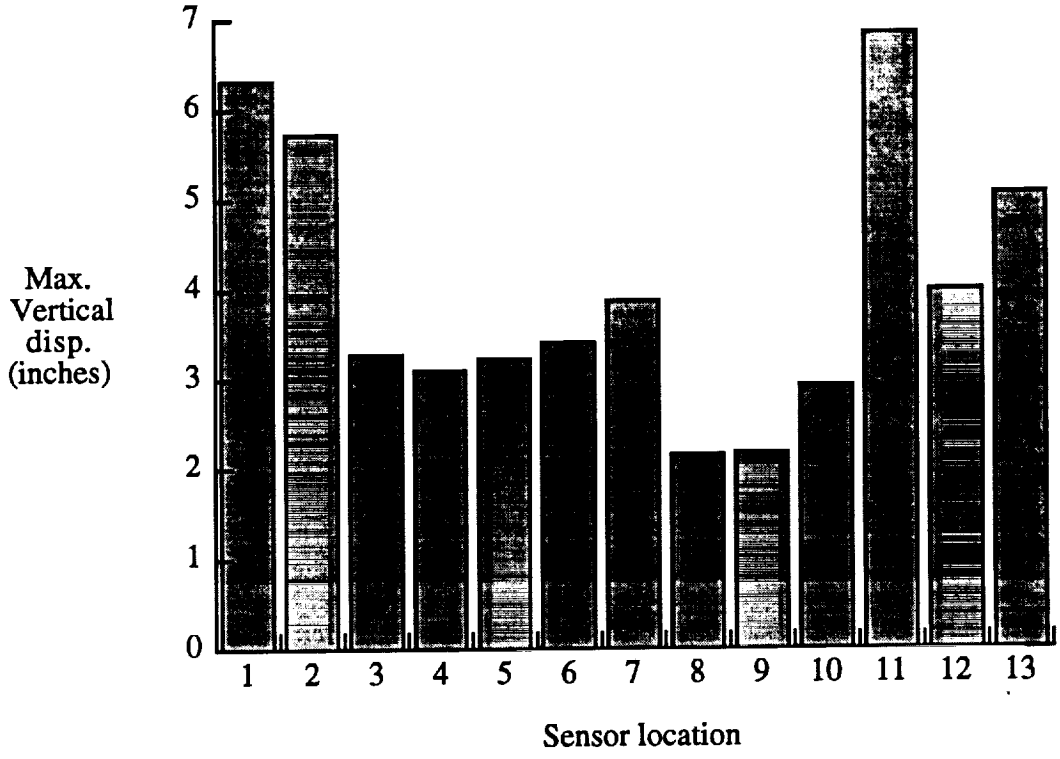

Figure 30. RTO maximum vertical displacement at 13 sensor locations

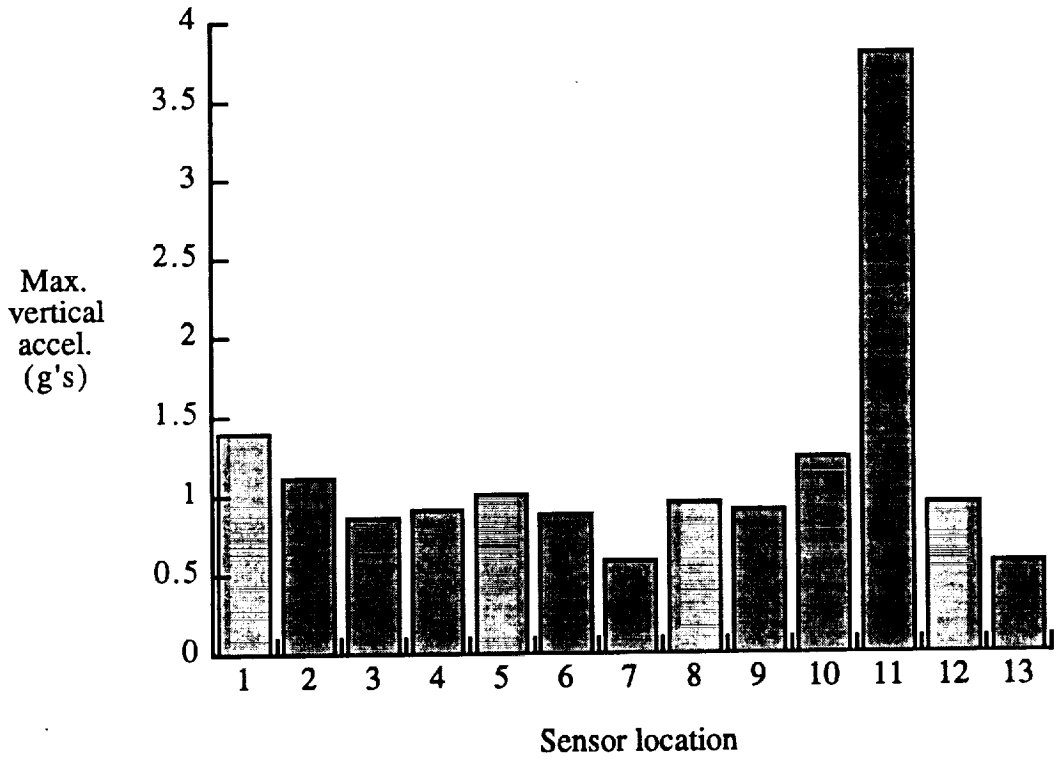

Figure 31. RTO maximum vertical accelerations at 13 sensor locations

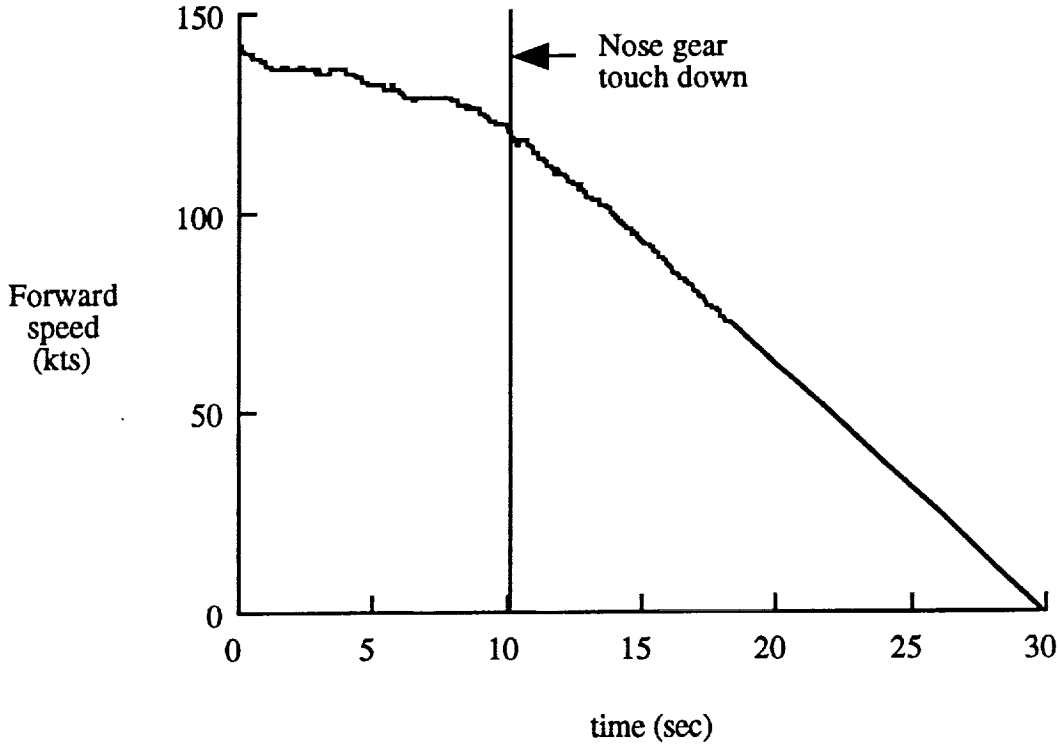

Figure 32. Landing forward speed profile

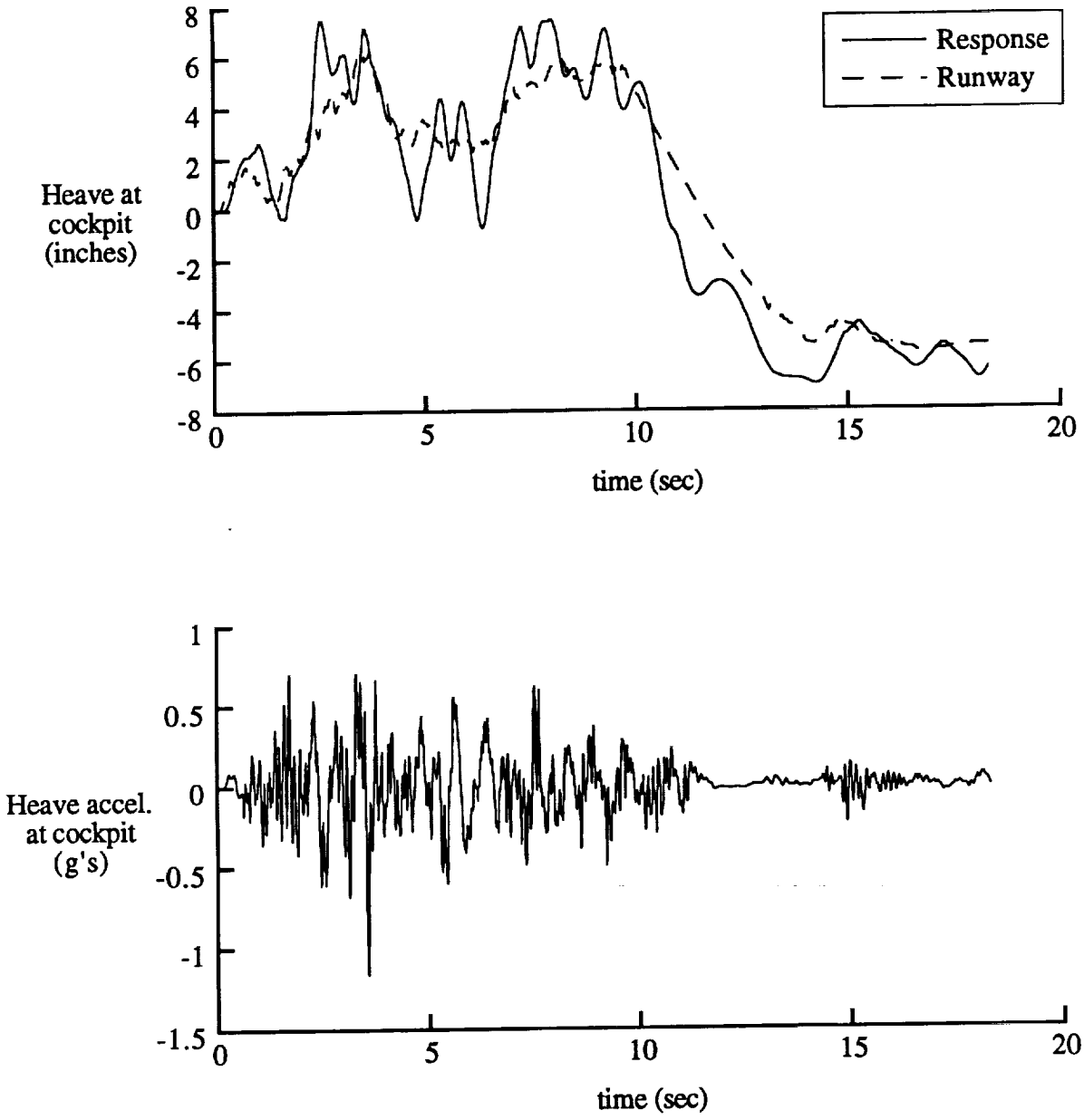

Figure 33. Landing vertical response at cockpit location

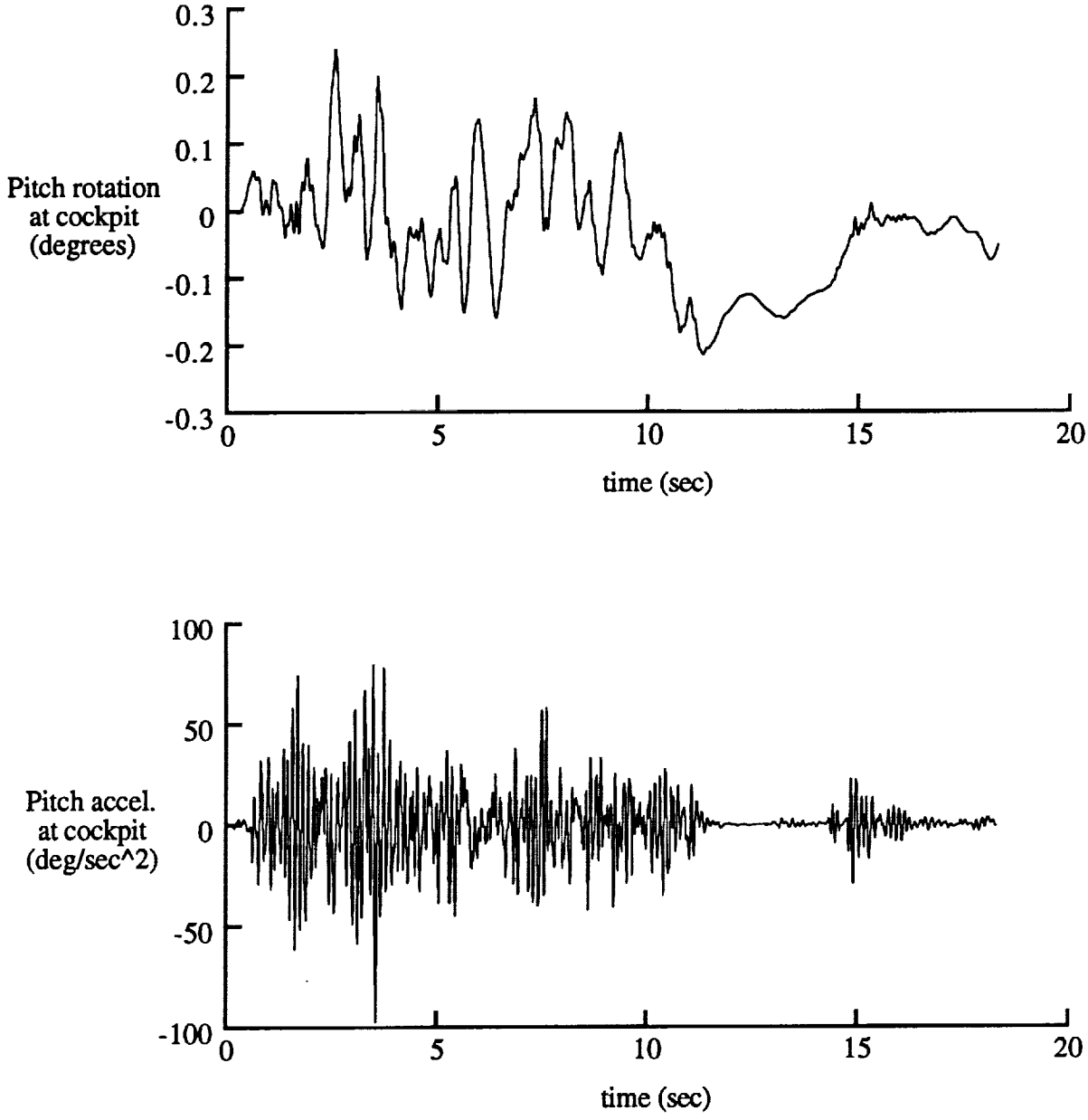

Figure 34. Landing pitch response at cockpit location

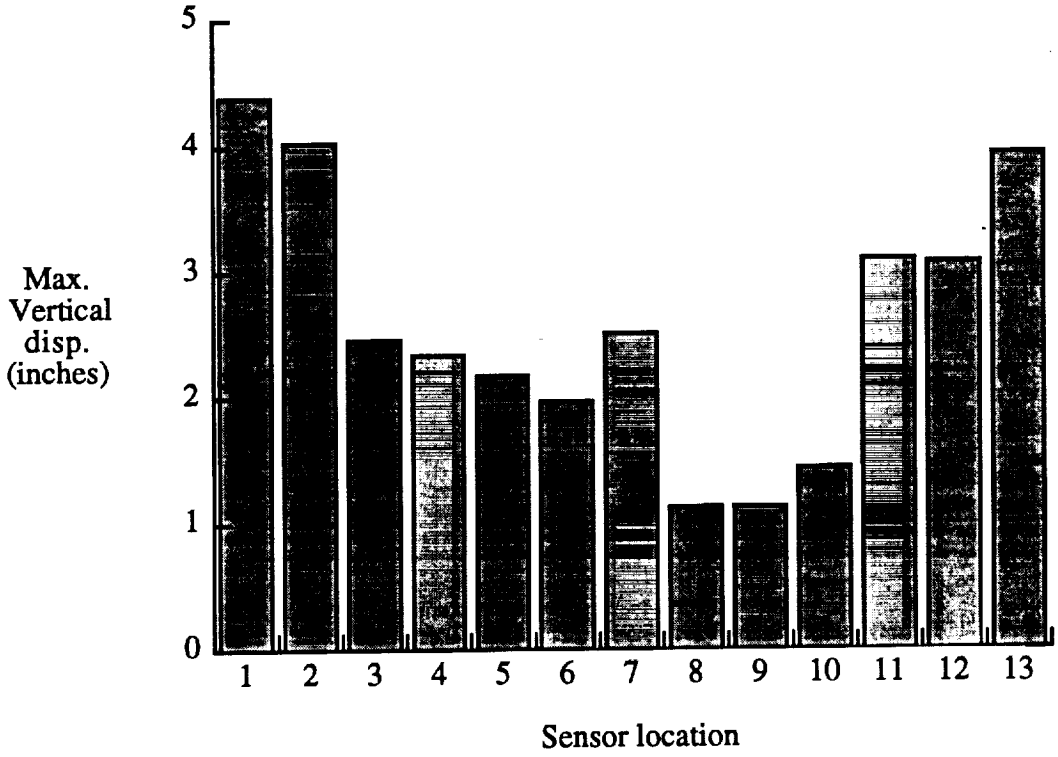

Figure 35. Landing maximum vertical displacements at 13 sensor locations

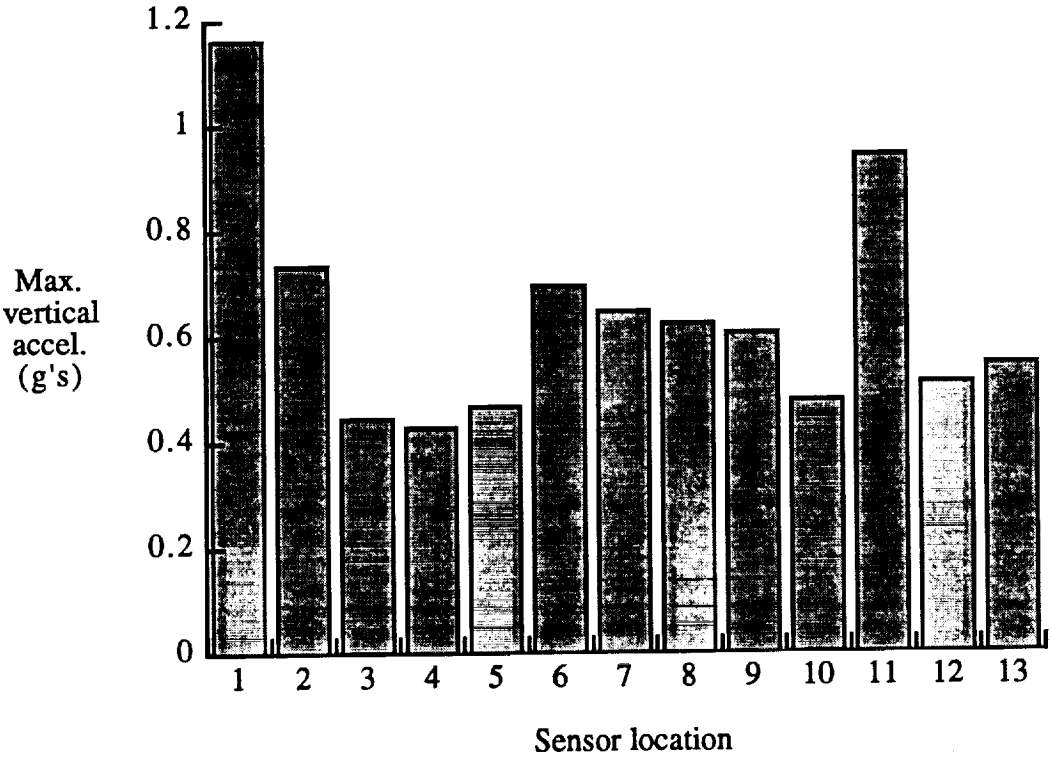

Figure 36. Landing maximum vertical accelerations at 13 sensor locations

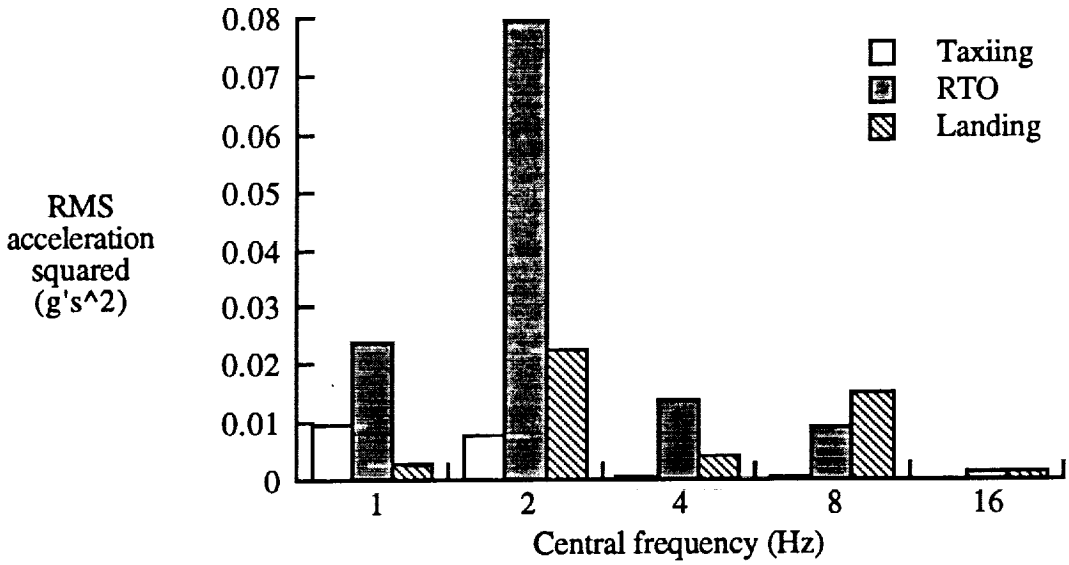

Figure 37. HSCT response at cockpit location during ground operations on the San Francisco runway

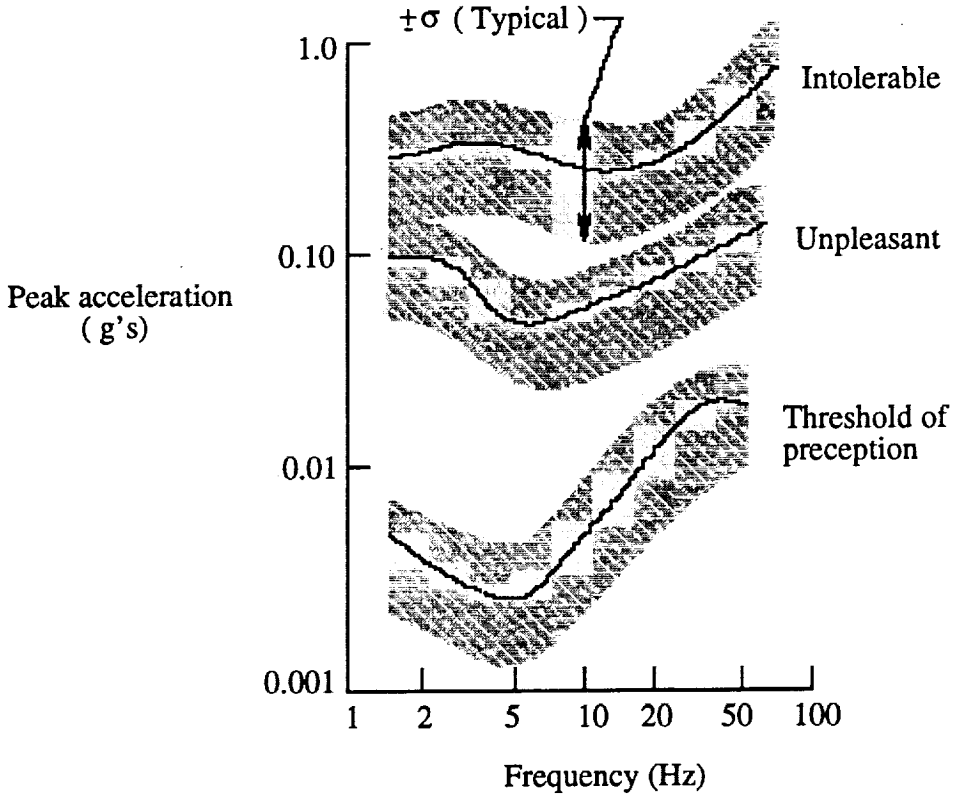

Figure 38. Human subjective response to vibration

REPORT DOCUMENTATION PAGE

Form Approved
OMB No. 0704-0188

1. AGENCY USE ONLY *(Leave blank)*	2. REPORT DATE	3. REPORT TYPE AND DATES COVERED
	December 1999	Technical Memorandum

4. TITLE AND SUBTITLE
Taxiing, Take-Off, and Landing Simulation of the High Speed Civil Transport Aircraft

5. FUNDING NUMBERS
WU 537-06-22

6. AUTHOR(S)
Mercedes C. Reaves and Lucas G. Horta

7. PERFORMING ORGANIZATION NAME(S) AND ADDRESS(ES)
NASA Langley Research Center
Hampton, VA 23681-2199

8. PERFORMING ORGANIZATION REPORT NUMBER
L-17901

9. SPONSORING/MONITORING AGENCY NAME(S) AND ADDRESS(ES)
National Aeronautics and Space Administration
Washington, DC 20546-0001

10. SPONSORING/MONITORING AGENCY REPORT NUMBER
NASA/TM-1999-209531

11. SUPPLEMENTARY NOTES

12a. DISTRIBUTION/AVAILABILITY STATEMENT
Unclassified–Unlimited
Subject Category 05 Distribution: Nonstandard
Availability: NASA CASI (301) 621-0390

12b. DISTRIBUTION CODE

13. ABSTRACT *(Maximum 200 words)*

The aircraft industry jointly with NASA is studying enabling technologies for higher speed, longer range aircraft configurations. Higher speeds, higher temperatures, and aerodynamics are driving these newer aircraft configurations towards long, slender, flexible fuselages. Aircraft response during ground operations, although often overlooked, is a concern due to the increased fuselage flexibility. This paper discusses modeling and simulation of the High Speed Civil Transport aircraft during taxiing, take-off, and landing. Finite element models of the airframe for various configurations are used and combined with nonlinear landing gear models to provide a simulation tool to study responses to different ground input conditions. A commercial computer simulation program is used to numerically integrate the equations of motion and to compute estimates of the responses using an existing runway profile. Results show aircraft responses exceeding safe acceptable human response levels.

14. SUBJECT TERMS	15. NUMBER OF PAGES
High-Speed Civil Transport; High-Speed Supersonic Transport; Supersonic transport; Simulation; Cockpit vibrations; Finite elements	48
	16. PRICE CODE: A03

17. SECURITY CLASSIFICATION OF REPORT	18. SECURITY CLASSIFICATION OF THIS PAGE	19. SECURITY CLASSIFICATION OF ABSTRACT	20. LIMITATION OF ABSTRACT
Unclassified	Unclassified	Unclassified	UL